IL-33 amplifies an innate immune response in the degenerating retina

Hongkang Xi,[1] Kenneth J. Katschke Jr,[1] Yun Li,[1] Tom Truong,[1] Wyne P. Lee,[1] Lauri Diehl,[2] Linda Rangell,[2] Jianhua Tao,[2] Rommel Arceo,[2] Jeffrey Eastham-Anderson,[2] Jason A. Hackney,[3] Antonio Iglesias,[5] Javier Cote-Sierra,[5] Justin Elstrott,[4] Robby M. Weimer,[4] and Menno van Lookeren Campagne[1]

[1]Department of Immunology, [2]Department of Pathology, [3]Department of Bioinformatics and Computational Biology, and [4]Department of Biomedical Imaging, Genentech, Inc., South San Francisco, CA 94080
[5]Roche Pharmaceutical Research and Early Development, Pharmacological Sciences, Roche Innovation Center Basel, CH-4070 Basel, Switzerland

Age-related macular degeneration (AMD), a leading cause of vision impairment in the ageing population, is characterized by irreversible loss of retinal pigment epithelial (RPE) cells and photoreceptors and can be associated with choroidal neovascularization. Mononuclear phagocytes are often present in AMD lesions, but the processes that direct myeloid cell recruitment remain unclear. Here, we identify IL-33 as a key regulator of inflammation and photoreceptor degeneration after retina stress or injury. IL-33+ Müller cells were more abundant and IL-33 cytokine was elevated in advanced AMD cases compared with age-matched controls with no AMD. In rodents, retina stress resulted in release of bioactive IL-33 that in turn increased inflammatory chemokine and cytokine expression in activated Müller cells. Deletion of ST2, the IL-33 receptor α chain, or treatment with a soluble IL-33 decoy receptor significantly reduced release of inflammatory mediators from Müller cells, inhibited accumulation of mononuclear phagocytes in the outer retina, and protected photoreceptor rods and cones after a retina insult. This study demonstrates a central role for IL-33 in regulating mononuclear phagocyte recruitment to the photoreceptor layer and positions IL-33 signaling as a potential therapeutic target in macular degenerative diseases.

Inflammation is traditionally considered a defense response triggered by infection or injury. However, inflammation can also be induced by tissue stress and malfunction in the absence of infection (or overt tissue damage; Chovatiya and Medzhitov, 2014). Examples of such stress-induced inflammatory responses are found at immune-privileged areas in the central nervous system and the retina. In age-related macular degeneration (AMD), lifelong exposure of the retina and the underlining retinal pigment epithelium (RPE) cells to various stimuli such as light, oxidative stress, and proteolysis enzymes can lead to aberrant neovascularization, RPE loss, and photoreceptor loss (de Jong, 2006). Neural retina loss is often associated with a sterile inflammatory response, which is in part characterized by accumulation of mononuclear phagocytes in the photoreceptor and photoreceptor outer-segment layers (Combadière et al., 2007; Sennlaub et al., 2013; Hu et al., 2015). Genetic or pharmacological inhibition of mononuclear phagocyte recruitment through CCR2 inhibition protects photoreceptors in models of retinal degeneration (Guo et al., 2012; Rutar et al., 2012; Sennlaub et al., 2013). The

factors that initiate recruitment of mononuclear phagocytes remain largely unknown.

As IL-1β and IL-18 have been implicated in immune and vascular responses in the retina (Lavalette et al., 2011; Doyle et al., 2012, 2014; Tarallo et al., 2012; Rivera et al., 2013), we set out to study a potential role for IL-33 in retina inflammation. IL-33 is a recently discovered cytokine of the IL-1 family (Schmitz et al., 2005) that binds to the heterodimeric receptor consisting of ST2 and IL1RAcP (Lingel et al., 2009). IL-33, a 30-kD cytokine that encodes a nuclear localization signal and a chromatin-binding element in its N-terminal domain and an IL-1–like cytokine domain in its C terminus (Liu et al., 2013) was originally identified as a nuclear factor expressed in high endothelial venules (NF-HEV; Baekkevold et al., 2003). IL-33 is primarily expressed in the nuclei of structural and lining epithelial and endothelial cells in the periphery, and in glia cells in the CNS and retina. IL-33 released from cells can be further potentiated through proteolytic processing by a variety of proteases (Lefrançais et al., 2012). How IL-33 is released from and processed by glia cells in the CNS and retina is unknown.

IL-33 has pleiotropic functions (Villarreal et al., 2014) and can act on multiple cell types, including innate helper cells, macrophages, dendritic cells, eosinophils, basophils, and

mast cells. Whereas initially characterized as a Th2 cytokine promoting type 2 inflammation (Schmitz et al., 2005; Gadina and Jefferies, 2007; Espinassous et al., 2009; Hueber et al., 2011), additional studies have shown that IL-33 in vivo is able to induce marked multiorgan cellular infiltrate of neutrophils, macrophages, dendritic cells, and eosinophils (Bessa et al., 2014); to recruit neutrophils to sites of infection (Alves-Filho et al., 2010); and to induce hematopoietic stem cell and progenitor cell mobilization in a CCR2-dependent way (Kim et al., 2014). Cigarette smoke, which is an important environmental risk factor for AMD, exacerbates an IL-33–dependent inflammatory response to infection of the lung (Kearley et al., 2015). In the CNS, IL-33 released from glia cells triggers infiltration of monocytes, which in turn contribute to a healing response after traumatic CNS injury (Gadani et al., 2015). Although IL-33 expression in mouse Müller cells has been reported (Pichery et al., 2012), its expression in the normal and affected human eye, its cellular targets, and its role in regulating inflammatory responses after retinal degeneration are not well understood.

Here, we demonstrate that IL-33 is expressed in the nucleus of Müller cells of the human macula. The number of IL-33^{+} Müller cells was increased in areas of retina atrophy compared with adjacent, unaffected areas, and levels of IL-33 were increased in vitreous from patients diagnosed with AMD compared with controls. IL-33 is released from Müller glia cells upon exposure of mice or rats to constant bright light, a condition that results in accumulation of toxic visual cycle products, loss of photoreceptors, and accumulation of mononuclear phagocytes to the outer retina (Rutar et al., 2012; Sennlaub et al., 2013). Using genetic and pharmacological tools, we demonstrate that release of IL-33 and autocrine activation of its receptor on Müller cells after retina injury is associated with recruitment of mononuclear phagocytes to the outer retina and photoreceptor loss.

RESULTS
IL-33 expression in the human macula
The macula is a specialized area of the human retina that is critical for high-resolution visual acuity. Reduced viability of RPE and photoreceptor cells in the macula as a result of life-long exposure to oxidative stress or toxic byproducts of the visual cycle can have important consequences for visual function (Jarrett and Boulton, 2012; Maeda et al., 2014). To determine if IL-33 expression is different in the macula compared with peripheral retina, dissected postmortem human retina (Fig. 1 A) was analyzed by RNA sequencing. The number of IL-33 transcripts were significantly increased in macula versus peripheral retina of normal donors (Fig. 1 B), whereas expression levels of other IL-1 cytokines, IL-1α, IL-1β, and IL-18 were either similar or decreased in the macula compared with the peripheral retina. To further determine the cellular source of IL-33 in human retina, seven eyes from human donors with no history of AMD were processed for immunohistochemistry. IL-33 was predominantly present in the nuclei of

vimentin^{+} Müller cells of the central retina, with significantly lower numbers of IL-33^{+} Müller cells in the peripheral retina (Fig. 1, C–F) in line with the RNA sequencing results. IL-33 was also expressed in the nucleus of a subpopulation of RPE cells, with slightly higher expression in the central compared with the peripheral retina (Fig. 1, D and E). The number of IL-33^{+} astrocytes (glial fibrillary acidic protein[+] [GFAP[+]]) in the retinal ganglion cell (RGC) layer, or the number of IL-33^{+} endothelial cells (plasmalemma vesicle associated protein[+] [PLVAP[+]]) of the choroid, was not different in the central compared with the peripheral retina.

In donors with a history of AMD, areas of RPE and photoreceptor cell loss, reminiscent of advanced dry AMD or geographic atrophy, were observed in the macula (Fig. 2, A and B). Using multimarker immunofluorescence, we found an increased number of IL-33^{+} Müller cells and Iba1^{+} myeloid cells in areas of RPE and photoreceptor atrophy as compared with adjacent areas with no retina degeneration (Fig. 2, A–C). The number of IL-33^{+} Müller cells in the AMD nonlesion area was significantly lower than those in the central retina of the controls, most likely due to the fact that the nonlesion areas are typically located in the peripheral retina where IL-33^{+} Müller cells are less abundant than in the central retina of non-AMD eyes (Fig. 1 D). Increased IL-33^{+} cells were also observed in the choroid of AMD lesion areas relative to controls or nonlesion areas (Fig. 2 C). None of the Iba1^{+} myeloid cells were positive for IL-33. In the vitreous of a subpopulation of AMD patients, IL-33 levels were significantly increased compared with non-AMD controls (macular hole and macular pucker; Fig. 2 D).

IL-33 is processed and released from Müller cells in vitro and in vivo
In the rodent retina, IL-33 was primarily expressed in vimentin^{+} Müller cells of the central and peripheral retina (Fig. 3 A), as previously described for the mouse retina (Pichery et al., 2012). Different from expression in humans, few IL-33^{+} cells with low expression were observed in RPE or choroid (Fig. 3 A). In the normal mouse retina, IL-33 mRNA and protein expression was at least 50-fold higher compared with other IL-1 family members (IL-1α, IL-1β, and IL-18; Fig. 3 B and not depicted). rMC-1, a Müller cell line obtained from rats exposed to bright light (Sarthy et al., 1998), was subsequently used to study the regulation of IL-33 release in vitro. rMC-1 Müller cells in culture displayed an activated phenotype as shown by expression of GFAP (not depicted; Sarthy et al., 1998). Subcellular fractionation of these cells identified expression of 30-kD pro–IL-33 and ~24- and ~19-kD C-terminal peptides in the nuclear fraction, whereas IL-33 p19 was the primary species expressed in the cytoplasm (Fig. 3 C). Exposure of rMC-1 cells to high glucose (25 mM), which activates the Müller cells (Sarthy et al., 1998; not depicted), significantly increased IL-33 secretion compared with cells cultured in low-glucose (5.5 mM) medium (Fig. 3 D). Western blotting analysis of the culture supernatant demonstrated a processed C-terminal 19-kD IL-33
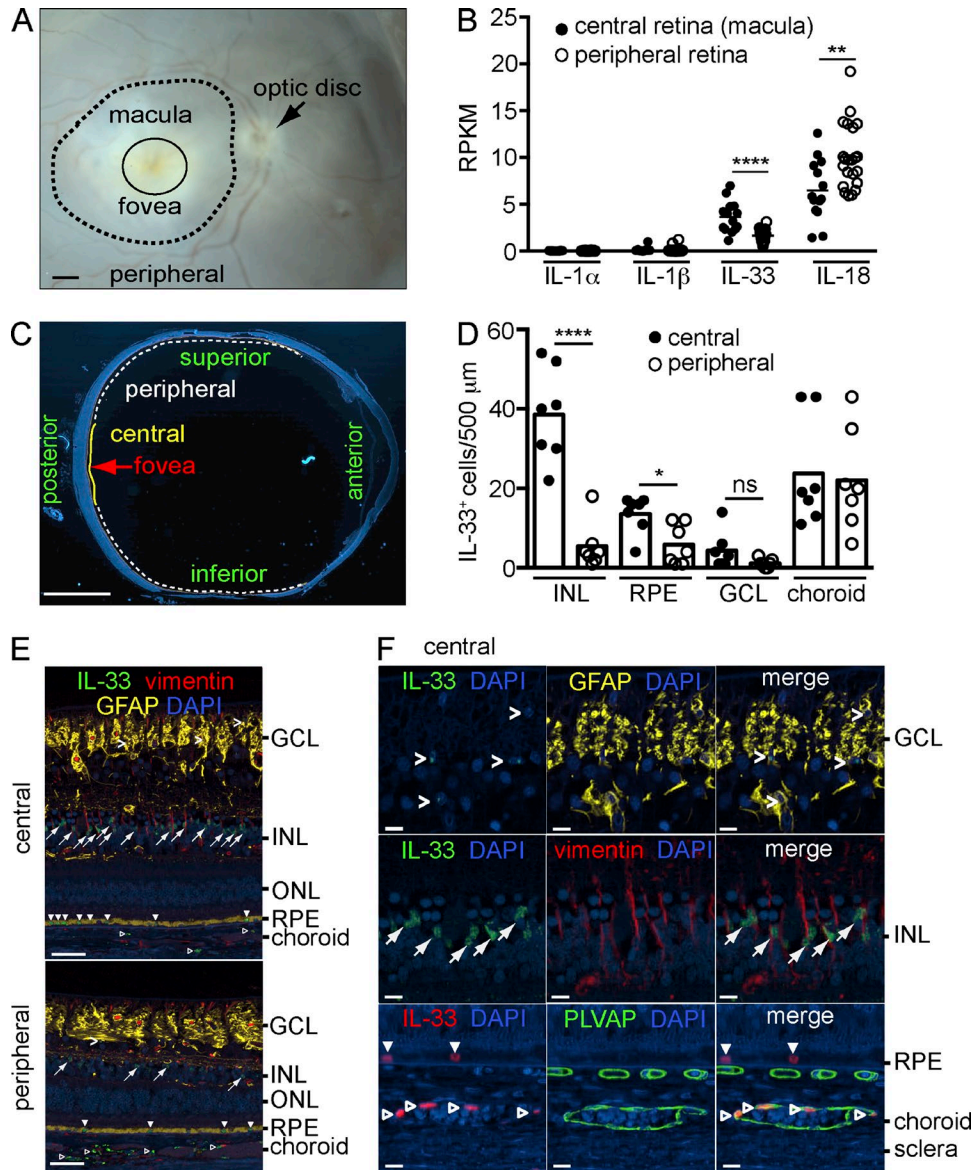
Figure 1. **Expression of IL-33 in Müller cells of the human macula.** (A) A representative stereoscope image of a human retina showing the areas of macula and peripheral retina dissected for RNA-sequencing. Bar, 1 mm. (B) RNA-sequencing analysis of IL-1α, IL-1β, IL-18, and IL-33 expression presented as reads per kilobase per million total reads (RPKM) in the macula ($n = 14$ eyes) and peripheral retina ($n = 22$ eyes) of control donor eyes. (C) Representative cross section of a human donor eye with central and peripheral areas for quantitative analysis indicated. Bar, 5 mm. (D) Quantification of IL-33^{+} cells in each retinal layer of central and peripheral areas from seven control donor eyes with age range of 67–89 yr (median age 84, five males and two females). (E) Representative images of immunohistochemical triple staining of IL-33 (green), vimentin (red), and GFAP (yellow) in a control eye from an 84-yr-old male donor. Angle brackets, IL-33^{+} astrocytes in the GCL; arrows, IL-33^{+} cells in the INL; filled arrowheads, IL-33^{+} cells in the RPE; open arrowheads, IL-33^{+} cells in the choroidal vasculature. Bars, 50 µm. (F) Representative high magnification images of IL-33^{+} cells in the GCL, INL, RPE, and choroid in the central area of a control donor eye. Shown are IL-33^{+} astrocytes (GFAP[+], angle brackets) and IL-33^{+} Müller cells (vimentin[+], arrows). IL-33^{+} endothelial cells (open arrowheads) of the choroidal vasculature are shown by IL-33 (red) and PLVAP (green) co-staining. Closed arrowheads, IL-33^{+} RPE. DAPI (blue), nuclear stain. Bars, 10 µm. GCL, ganglion cell layer; INL, inner nuclear layer; ONL, outer nuclear layer. *, P < 0.05; **, P < 0.01; ****, P < 0.0001; ns, nonsignificant; unpaired two-tailed Student's t tests.

protein as the only secreted IL-33 species (Fig. 3 D). High glucose stimulation up to 72 h didn't induce significant increase of PI[+] or Annexin V^{+} cells (Fig. 3 D) indicating that increased IL-33 p19 secretion in high glucose medium was not associated with reduced cell viability. In sum, we have demonstrated that IL-33 is expressed in both human and rodent Müller cells with predominant localization to the nucleus and that IL-33 p19 can be released from activated rat Müller cells in culture.
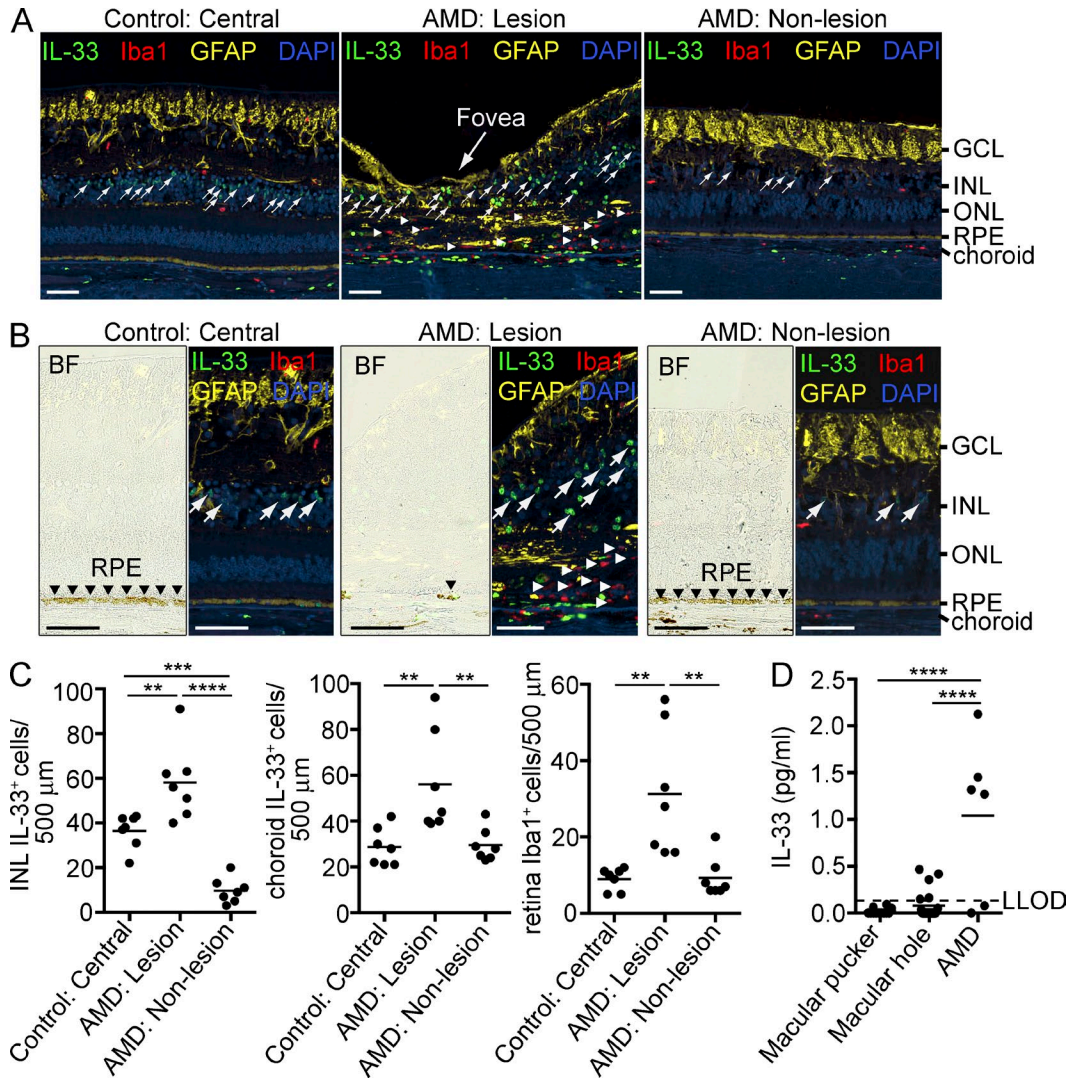
Figure 2. **Increased expression of IL-33 in areas of macular degeneration.** (A) Immunohistochemical triple staining of IL-33 (green), Iba1 (red), and GFAP (yellow) in the central retina of a control donor eye from an 84-yr-old male with no history of ocular diseases and from an eye of an 82-yr-old female donor diagnosed with AMD. Numbers of IL-33^{+} Müller cells and mononuclear phagocytic cells (Iba1^{+} cells) were quantified in areas of retina degeneration (AMD: Lesion), adjacent areas of the same donor that did not exhibit retina degeneration (AMD: Non-lesion), and the central retina of the control donor eye (Control: Central). Arrows, IL-33^{+} cells in the INL; arrowheads, Iba1^{+} cells in the subretinal space. DAPI (blue), nuclear stain. Bars, 50 µm. (B) High magnification images representing immunochemistry of IL-33 (green), Iba1 (red), and GFAP (yellow) in the central retina of a control eye and lesion and nonlesion areas of an AMD eye. The bright-field (BF) images show RPE loss in the AMD lesion site. Bars, 50 µm. (C) IL-33^{+} cells in the INL and the choroid and Iba1^{+} cells in the retina were counted along an ~500-µm section within the central retina of seven control donors aged 67–89 yr (median age 84) and lesion and nonlesion areas of eyes from seven AMD donors aged 82–92 yr (median age 86). (D) IL-33 levels in the vitreous from AMD and control patients. IL-33 concentrations in vitreous samples obtained from AMD patients ($n = 6$, one male and five females, age 68–91, median age 79) and control patients with macular pucker ($n = 12$, three males and nine females, age 56–79, median age 72) and macular hole ($n = 21$, 5 males and 16 females, age 46–75, median age 65) were measured by ELISA. **, $P < 0.01$; ***, $P < 0.001$; ****, $P < 0.0001$; one-way ANOVA with Tukey's post-tests. Horizontal bars represent means.

We next asked if IL-33 could be secreted from Müller cells after activation in vivo. Constant exposure of Sprague-Dawley rat to bright light (1,200 lux) for several days (constant light exposure [CLE]) resulted in progressive loss of rods and cones in parallel with increased activation of Müller cells, microglia, and macrophages (LaVail et al., 1992). After CLE, the number of terminal dUTP nick end-labeling (TUNEL)–positive cells in the ONL increased, along with loss of rods and cones (unpublished data). Rare TUNEL^{+} cells were observed in the INL where the Müller cells reside. To determine if IL-33 is released by cells in vivo, we collected vitreous humor at various time points after CLE. IL-33 levels in normal rat vitreous were ~1 ng/ml. IL-33 concentrations increased twofold in light-activated eyes, reaching a
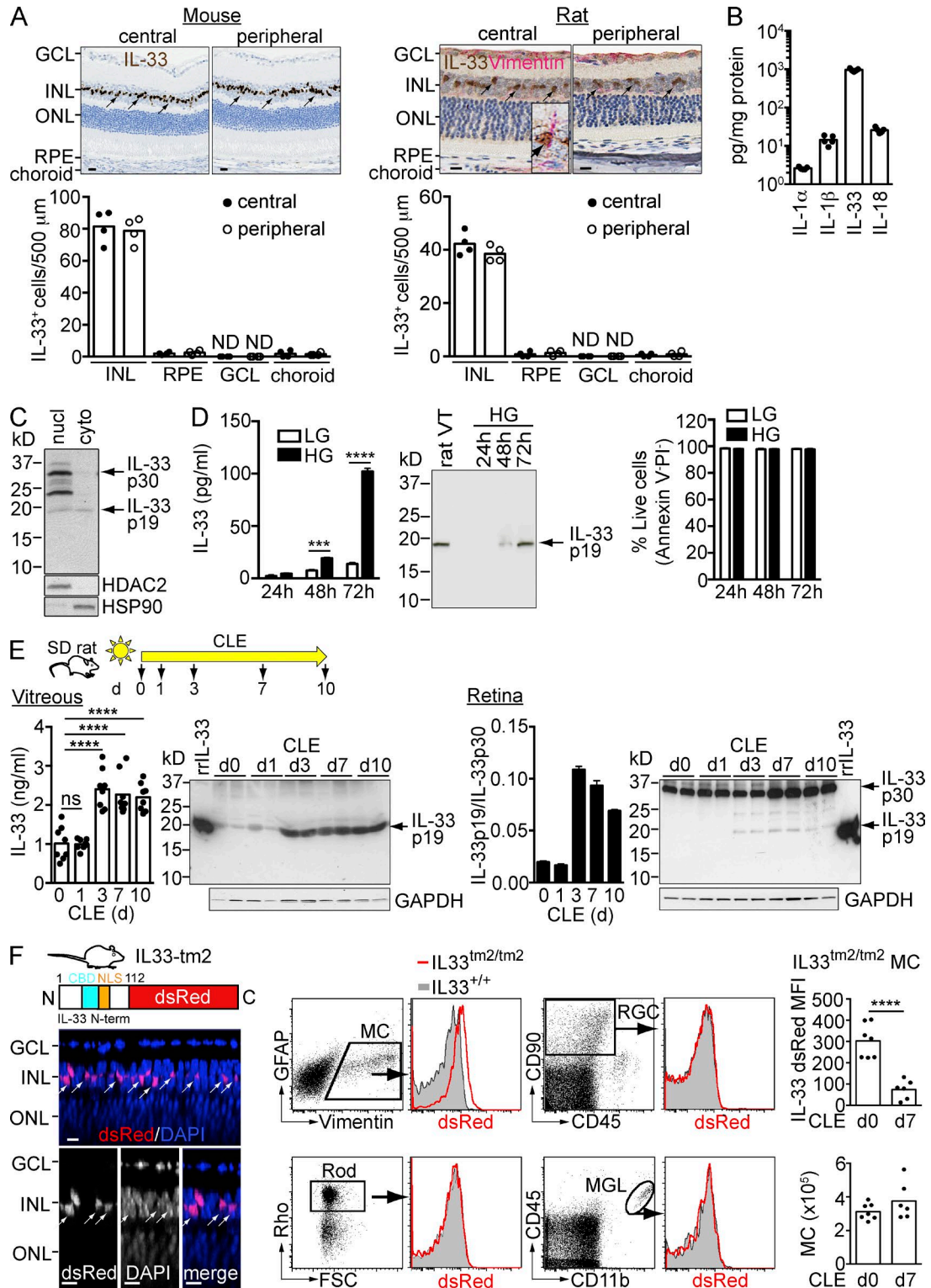
Figure 3. **IL–33 C terminus is released from Müller cells in vitro and in vivo after phototoxic stress.** (A) Immunohistochemical staining of IL-33 (brown) in BALB/c mouse and Sprague-Dawley (SD) rat retina. The rat retina was co-stained with vimentin (red). Arrows, IL-33+ Müller cells. (inset) An IL-33+ vimentin+ Müller cell. IL-33+ cells in the INL, RPE, GCL, and choroid in the central and peripheral retina were counted along a ∼500-µm section. Bars, 10 µm. ND, not detected. (B) Expression of IL-1 family genes (IL-1α, IL-1β, IL-33, and IL-18) in the retina of BALB/c mice was measured by ELISA. Each data point represents an individual mouse (*n* = 5). (C) Western blotting of IL-33 expression in the nuclear (nucl) and cytoplasmic (cyto) fraction of rMC-1 cells. (D) ELISA and

plateau at day 3 (Fig. 3 E). Western blot analysis confirmed that the processed C-terminal 19-kD peptide, identical in size to the IL-33 fragment released from rMC-1 cells in culture (Fig. 3 D), was the predominant IL-33 species present in vitreous before and after CLE (Fig. 3 E, left). Full-length IL-33 p30 was the primary species in the retina with an increased presence of the 19-kD processed IL-33 starting at day 3 after light exposure (Fig. 3 E, right) with a time-course similar to IL-33 p19 expression in vitreous. To determine whether the increased presence of IL-33 p19 in the light-injured retina and rMC-1 cells cultured in high-glucose medium was caused by increased transcription of an alternative splice variant of IL-33, RT-PCR was performed using PCR primers spanning the 5′ UTR (exon 1) and the stop codon (exon 9) of IL-33. Only full-length IL-33 transcript was detected in all conditions (unpublished data). Although this suggests that IL-33 p19 was generated by proteolysis rather than by alternative splicing, the protease responsible for IL-33 processing has yet to be identified and is the focus of ongoing studies.

We observed loss of native IL-33 from rat Müller cells after light exposure (unpublished data). To determine the regulation of IL-33 protein expression in Müller cells in vivo, we used genetically engineered IL33[tm2/tm2] mice (Bessa et al., 2014) in which the N terminus of IL-33, containing the nuclear localization signal and the chromatin-binding domain, was fused to a dsRed reporter. In retina from IL33[tm2/tm2] mice, IL-33 N-term–dsRed localized primarily to the nucleus of Müller cells located in the inner nuclear layer of the retina (Fig. 3 F, left), similar to the localization of native full-length IL-33 (Fig. 3 A). FACS analysis of the IL33[tm2/tm2] retina confirmed the selective expression of IL-33 N-term–dsRed in Müller cells (Fig. 3 F, middle). A significant loss of IL-33–dsRed from live Müller cells was observed after CLE without loss of Müller cells (Fig. 3 F, right), which suggests release of IL-33 C terminus from Müller cells in the absence of Müller cell loss.

ST2 is expressed on activated Müller cells and contributes to photoreceptor loss

IL-33 triggers MyD88-mediated signaling after binding to its heterodimeric receptor, ST2/IL1RAcP (Schmitz et al., 2005).

Retina transcripts encoding trans–membrane ST2 (ST2L) and a splice variant of ST2 that lacks the trans–membrane domain (sST2) increased 4–10-fold after CLE of BALB/c mice, peaking at day 3 (Fig. 4 A). Flow cytometry analysis in parallel samples identified activated (GFAP^{+}) Müller cells as the primary source of trans–membrane ST2 in the light-exposed retina (Fig. 4 B, top), whereas ST2 was not detectable on Müller cells before light exposure (unpublished data). ST2 was not detected on CD45^{lo}CD11b^{+} microglia (Fig. 4 B, bottom), RGCs, or photoreceptors (not depicted). We next determined whether IL-33 binding to ST2 impacts photoreceptor survival after CLE. Spectral domain optical coherence tomography (SD-OCT) demonstrated sparing of retina in ST2^{−/−} versus ST2^{+/+} mice after 7 d (Fig. 4 C) and 14 d (not depicted) of CLE. Flow cytometry of total retina further confirmed that rods, cones, and ganglion cells (unpublished data) were protected in ST2^{−/−} versus ST2^{+/+} mice during CLE for 14 d (Fig. 4 D). Morphometric analysis on sections through the eye showed significant protection of photoreceptors in ST2^{−/−} mice after retinal phototoxic injury in both the superior and inferior halves of the retina (Fig. 4 E). Electroretinograms (ERGs) were recorded at day 7 after CLE and demonstrated improved a- and b-wave responses in ST2^{−/−} versus ST2^{+/+} mice reflecting improved retina function (Fig. 4 F). In contrast to ST2^{−/−} mice, retinas of albino (BALB/c) IL-1R1^{−/−} and IL-18R1^{−/−} mice that lack the receptors for IL-1α, IL-1β, and IL-18, respectively, were not protected compared with WT littermates after CLE (unpublished data).

To further determine if pharmacological blockade of ST2–IL-33 interaction protects photoreceptors, mice were treated with a recombinant adeno-associated virus (AAV) expressing soluble ST2 (AAV-sST2) followed by CLE. Blocking activity of sST2 was verified in IL-33–stimulated BM-derived mast cells (BMMCs; unpublished data). ELISA and Western blotting confirmed the expression of sST2 in AAV-infected HEK293 cells (unpublished data). Subretinal injection of AAV-sST2 led to high level expression of sST2 in the retina and RPE (Fig. 5 A). Light-exposed mice treated with AAV-sST2, but not control vector, showed protection of rods, cones, and ganglion cells (Fig. 5 B and not depicted). Based on these results, IL-33 binding to its signaling receptor

Western blotting analysis of IL-33 secretion from rMC-1 cells cultured in high-glucose (HG) and low-glucose (LG) containing medium. rat VT, rat vitreous. Cell viability was assessed by FACS analysis of Annexin V and PI staining. Live cells were gated as Annexin V[−] PI[−]. Data shown are means ± SEM of triplicate wells. (E) Expression and secretion of IL-33 p19 in rat vitreous and retina after CLE. SD rats were exposed to bright light for up to 10 d. IL-33 expression in the vitreous and retina was analyzed by ELISA and Western blotting. The ratio of IL-33 p19 versus IL-33 p30 in the retina was quantitated with Image J software. A recombinant rat IL-33 protein (rrIL-33; aa 109–264, ∼18 kD) was used as the positive control for the detection Ab. Each data point in ELISA represents an individual mouse (n = 8/time point). (F) IL33[tm2/tm2] mice with intact IL-33 nuclear localization sequence (NLS) and chromatin-binding domain (CBD), but with the IL-33 cytokine domain replaced by dsRed show localization of IL-33 N-term–dsRed in nuclei of Müller cells in the INL. Images shown are Z-section views of confocal images of an IL33[tm2/tm2] retina flat-mount. Arrows, IL-33^{+} Müller cells. Bars, 5 µm. Flow cytometry analysis of IL33[tm2/tm2] retina with expression of IL-33 in Müller cells (MC) but not in rods, ganglion cells (RGC), or microglia (MGL). dsRED mean fluorescent intensity (MFI) of IL33[tm2/tm2] Müller cells, as well as Müller cell numbers at d0 and d7 of CLE, were measured by flow cytometry. Data represent the MFI of dsRed in IL33[tm2/tm2] mice normalized to that of IL33^{+/+} mice. Each data point represents an individual mouse (n = 6–7/group). Rho, rhodopsin; FSC, forward scatter. ***, P < 0.001; ****, P < 0.0001; ns, nonsignificant; two-way ANOVA with Bonferroni's post-test (D), one-way ANOVA with Dunnett's post-test (E), or unpaired two-tailed Student's t test (F). Data in B–F are representative of at least two experiments with similar results.
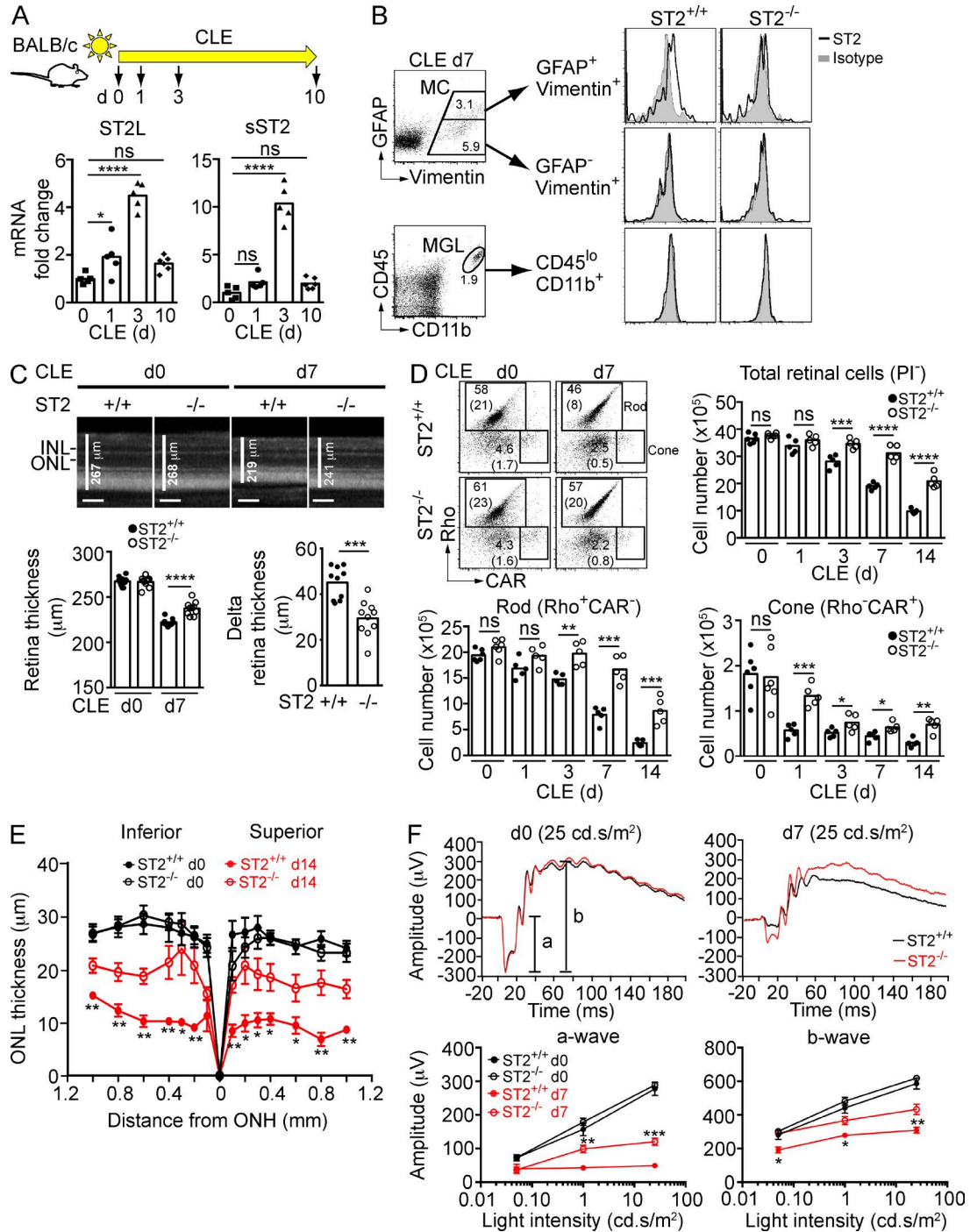
Figure 4. **ST2 is expressed on activated Müller cells after phototoxic stress and blocking ST2 signaling protects photoreceptors.** (A) Expression of membrane-bound (ST2L) and soluble (sST2) ST2 following CLE. Retina RNA from BALB/c mice exposed to light for various days was analyzed by qPCR using probes specific for ST2L and sST2, and normalized to 18s rRNA. ST2 expression in nonexposed mice (d0) was set as 1. Each data point represents an individual mouse (n = 5–6/time point). (B) Expression of ST2 on activated (GFAP^{+}vimentin^{+}), resting (GFAP^{−}vimentin^{+}) Müller cells (MC), and microglia (CD45^{lo}CD11b^{+}; MGL) after 7 d light exposure. (C) OCT analysis of retina thickness at baseline (d0) and after 7 d exposure to light in ST2^{+/+} and ST2^{−/−} mice. Delta retina thickness was calculated by subtracting retina thickness of day 0 by that of day 7 for each mouse (n = 10/genotype). Bars, 100 µm. (D) Rods and cones in ST2^{+/+} and ST2^{−/−} mice were quantified by flow cytometry. FACS plots indicate gating strategy and percentages, as well as absolute numbers (×10^{5}; between parentheses) of rods and cones in ST2^{+/+} and ST2^{−/−} mice. Each data point represents an individual mouse (n = 5–6/group). Rho, rhodopsin; CAR, cone arrestin. (E) Morphometric analysis of ONL thickness of ST2^{+/+} and ST2^{−/−} mice at baseline (d0) and after 14 d exposure to light plotted as a function of distance from the optic nerve head (ONH). Data shown are means ± SEM (n = 5–7/group). (F) ERG of ST2^{+/+} and ST2^{−/−} mice at baseline (d0) and after 7 d

ST2–IL1RAcP results in a pathogenic response that leads to photoreceptor loss in the light-exposed retina.

IL–33 increases recruitment of myeloid cells to the photoreceptor layer

To determine which pathways downstream of ST2–IL1RAcP signaling cause photoreceptor loss, we performed microarray analysis on ST2$^{+/+}$ and ST2$^{-/-}$ mice exposed to constant light for 3 d. After CLE, the retinas of ST2$^{+/+}$ mice displayed an overall increase in signatures of inflammation compared with ST2$^{-/-}$ mice, including CCL2, CCL4, IL-1β, IRF1, IRF7, and STAT3 (Fig. S1, Table S1, and Table S2). Real-time PCR confirmed increased expression of CCL2, IL-1β, and IL-6 after CLE, with significantly reduced expression in ST2$^{-/-}$ mice compared with ST2$^{+/+}$ mice (Fig. 6 A). Consistent with the mRNA expression data, CCL2 protein expression in the retina was reduced in ST2$^{-/-}$ compared with ST2$^{+/+}$ mice after CLE. We next determined whether IL-33 induces CCL2 expression in Müller cells. In line with our observation in vivo, rMC-1 cells, expressing the Müller cell activation marker GFAP, constitutively express trans-membrane, surface-exposed ST2 (Fig. 6 B). When stimulated with recombinant IL-33, rMC-1 cells showed a dose-dependent increase in CCL2 expression, which was blocked with IL-33 TRAP (Fig. 6 B), confirming that IL-33 signals through ST2 on Müller cells. In addition to IL-33, rMC-1 cells expressed and secreted CCL2 when cultured in high-glucose medium (Fig. 6 C). CCL2 expression was significantly reduced in rMC-1 cells treated with IL-33 TRAP compared with vehicle-treated cells. This demonstrates that Müller cells in culture release bioactive IL-33 that in turn can induce CCL2 through autocrine activation. CD45^{lo}CD11b^{+} myeloid cells in the retina express CCR2 (Fig. 6 D), the receptor for CCL2. To determine if IL-33 had any effect on myeloid cell distribution in the retina, we quantified Iba1^{+} myeloid cells in each retinal layer before and after CLE in ST2$^{+/+}$ and ST2$^{-/-}$ mice. Before light exposure, Iba1^{+} cells populated the inner plexiform layer (IPL) and outer plexiform layer (OPL) with very few cells in the ONL, outer segment (OS), and ganglion cell layer (GCL; Fig. 6 E). After CLE for 14 d, Iba1^{+} cells accumulated in the ONL, OS, and GCL with concomitant reduction of Iba1^{+} cells in the OPL and IPL in ST2$^{+/+}$ mice. ST2$^{-/-}$ mice showed 40–50% reduction of Iba1^{+} cells in the ONL and OS, and a 50% increase in Iba1^{+} cells in the OPL compared with ST2$^{+/+}$ mice (Fig. 6 F). Thus, after CLE, ST2–IL1RAcP signaling increased CCL2 production, increased presence of Iba1^{+} myeloid cells in the outer retina layers, and induced loss of photoreceptor rods and cones. These results are in line with a previously proposed role for Müller cell–secreted CCL2 in promoting myeloid cell presence in the ONL and promoting photoreceptor death after light–injury or retinal detachment (Nakazawa et al., 2007; Rutar et al., 2011, 2012, 2015). To determine whether IL-33/ST2-induced photoreceptor loss upon light exposure is mediated by infiltrating myeloid cells, we depleted peripheral monocytes in ST2$^{+/+}$ and ST2$^{-/-}$ mice with clodronate and quantified the number of photoreceptors and ganglion cells after 7 d of CLE. Clodronate treatment depleted Ly6C^{hi}CD115^{+} and Ly6C$^{lo/-}$CD115^{+} peripheral monocytes by >80% and >70%, respectively (unpublished data). Monocyte depletion resulted in protection of rods, cones, and RGCs after CLE in ST2$^{+/+}$ mice (Fig. 6 G). However, ST2 deficiency did not provide further protection of photoreceptors when monocytes were depleted, indicating that infiltrating myeloid cells mediate IL-33/ST2-induced photoreceptor loss.

To determine if increased IL-33 release from Müller cells has a pathogenic role, we used a genetically modified mouse in which the N-terminal nuclear localization signal and chromatin-binding domain of IL-33 were replaced with dsRed (IL33$^{tm1/tm1}$ mice; Bessa et al., 2014; Fig. 7 A). Similar to IL33$^{tm2/tm2}$ mice, IL33$^{tm1/tm1}$ mice showed dsRed expression selectively in Müller cells of the neural retina. However, in contrast to IL33$^{tm2/tm2}$ mice, where dsRed is anchored to the nucleus via the IL-33 N terminus, replacing the IL-33 N terminus with dsRed in IL33$^{tm1/tm1}$ mice prevented IL-33 anchoring to the nucleus, resulting in release of IL-33 C terminus in cytoplasm of Müller cell processes spanning the inner nuclear layer. Compatible with IL-33 transcription remaining under control of the endogenous promoter (Bessa et al., 2014), IL-33 mRNA in the retina was unaltered in IL33$^{tm1/+}$ and IL33$^{tm1/tm1}$ mice compared with IL33$^{+/+}$ littermate mice, whereas IL-33 protein in serum and retina was elevated (Fig. 7 A). In agreement with a pathogenic role of the IL-33–ST2 axis, retina from the IL33$^{tm1/+}$ and IL33$^{tm1/tm1}$ mice showed increased CCL2 and IL-6 expression and loss of photoreceptor cones and ganglion cells when the mice expressed the ST2 receptor chain (ST2$^{+/-}$ background; Fig. 7 B). CCL2 and IL-6 expression and retinal cell loss were reversed to control values in IL33$^{tm1/+}$ and IL33$^{tm1/tm1}$ mice lacking ST2 (Fig. 7 B). This indicates that IL-33, when deprived of the capacity to localize to the nucleus, is released from the cell and induces ST2-dependent cytokine and chemokine release along with death of retinal cells.

Circulating monocytes are required for IL-33/ST2–induced photoreceptor cell loss after RPE disruption

RPE performs a critical role in photoreceptor homeostasis through ingestion and recycling of photoreceptor outer segments, inactivating toxic visual cycle products, and fulfilling the metabolic demand of the retina. Importantly, RPE also

---

CLE. (top) Representative ERG recordings at 25 cd/s/m^2 light intensity of baseline and after 7 d CLE. Data shown are means ± SEM (n = 10/genotype). *, P < 0.05; **, P < 0.01; ***, P < 0.001; ****, P < 0.0001; ns, nonsignificant; one-way ANOVA with Dunnett's post-tests (A), two-way ANOVA with Tukey's post-tests (F), or unpaired two-tailed Student's t tests (C, D, and E). Data are representative of at least two independent experiments with similar results.
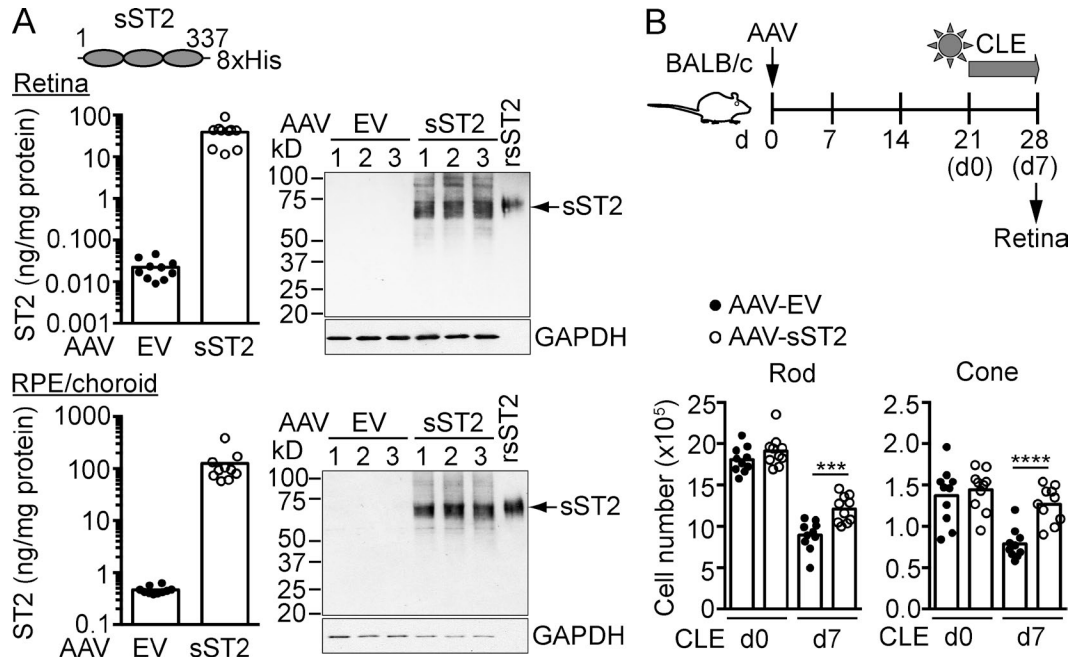
Figure 5. **Soluble ST2 protects photoreceptors from phototoxic stress.** (A) BALB/c mice were subretinally injected with an AAV (AAV2/5) expressing soluble ST2 (AAV-sST2) or AAV empty vector (AAV-EV) which served as a negative control. Expression of sST2 in the retina and RPE/choroid 3 wk after infection was analyzed by ELISA and Western blotting (10 μg of retina lysates and 3 μg of RPE/choroid lysates). rsST2, recombinant soluble ST2-His. (B) Mice were subretinally injected with AAV-sST2 or AAV-EV and exposed to light 3 wk after infection. Rods and cones were quantified by flow cytometry before (d0) and after 7 d CLE. Each data point represents an individual mouse (n = 10/group). ***, P < 0.001; ****, P < 0.0001; unpaired two-tailed Student's t tests. Data are representative of two independent experiments with similar results.

maintains the outer blood–retinal barrier (Strauss, 2005). Loss of RPE cells has been proposed to be causal to photoreceptor loss in both wet and dry forms of AMD (Bhutto and Lutty, 2012). Sodium iodate ($NaIO_3$) is an oxidizing compound that irreversibly affects RPE cell survival upon systemic administration (Carido et al., 2014) and offers the opportunity to study the role of retinal pathways important in photoreceptor loss secondary to RPE cell death.

Systemic administration of $NaIO_3$ resulted in elimination of the majority of RPE cells in the central retina by day 3. This was paralleled by loss of ONL photoreceptor cells, activation of Müller cells (Fig. 8 A), and the increased presence of 19-kD processed IL-33 in the neural retina, peaking at day 3 after treatment (Fig. 8 B). Treatment with $NaIO_3$ also resulted in a >1,500-fold increase in CCL2, which was reduced by ~35% in mice lacking ST2 (Fig. 8 C). Given that IL-33 stimulation of Müller cells induces CCL2, we determined whether blockade of IL-33 would affect the number of myeloid cells in the retina. Treatment of $ST2^{+/+}$ mice with $NaIO_3$ resulted in a >20 fold increase in $CD45^{hi}$ $CD11b^+CCR2^+$ mononuclear phagocytes in the retina, peaking at day 3. $ST2^{-/-}$ mice showed a ~70% and ~50% decrease in macrophage cell numbers at day 3 and 7, respectively, after $NaIO_3$ treatment (Fig. 8 D). In contrast, numbers of $CD45^{lo}$ $CD11b^+$ microglia dropped over fivefold in both $ST2^{+/+}$ and $ST2^{-/-}$ mice at day 3 after $NaIO_3$ treatment and did not re-

cover at day 7 (unpublished data). Immunohistochemistry analysis of $Iba1^+$ cells showed ~50–60% reduction of $Iba1^+$ myeloid cells in OS and ONL in $ST2^{-/-}$ mice compared with $ST2^{+/+}$ mice at day 3 after $NaIO_3$ treatment (Fig. 8 E). The neural retina of $ST2^{-/-}$ mice was protected after $NaIO_3$ treatment, as shown by significantly thicker retina in $ST2^{-/-}$ mice compared with $ST2^{+/+}$ mice at day 7 after $NaIO_3$ treatment (Fig. 8 F, top and middle). Significant sparing of rods, cones (Fig. 8 F, bottom), and retinal ganglion cells (not depicted) was further demonstrated by FACS analysis. In contrast to $ST2^{-/-}$ mice, the retina of $IL-1R1^{-/-}$ or $IL-18^{-/-}$ mice was not protected compared with WT mice after $NaIO_3$ treatment (unpublished data).

To determine if mononuclear phagocytes are required for IL-33–induced photoreceptor loss in this model, we depleted peripheral monocytes in $ST2^{+/+}$ and $ST2^{-/-}$ mice with clodronate before $NaIO_3$ treatment and quantified the number of photoreceptors and ganglion cells at day 3. Successful depletion of $Ly6C^{hi}CD115^+CCR2^+$ and $Ly6C^{lo/-}CD115^+CCR2^+$ peripheral monocytes and $CD45^{hi}CD11b^+CCR2^+$ retinal mononuclear phagocytes was confirmed by flow cytometry (not depicted and Fig. 8 G). Myeloid cell depletion resulted in protection of the neural retina after $NaIO_3$-induced RPE cell loss (Fig. 8 G). Similar to the results from monocyte depletion experiments in CLE, loss of ST2 did not protect photoreceptors after
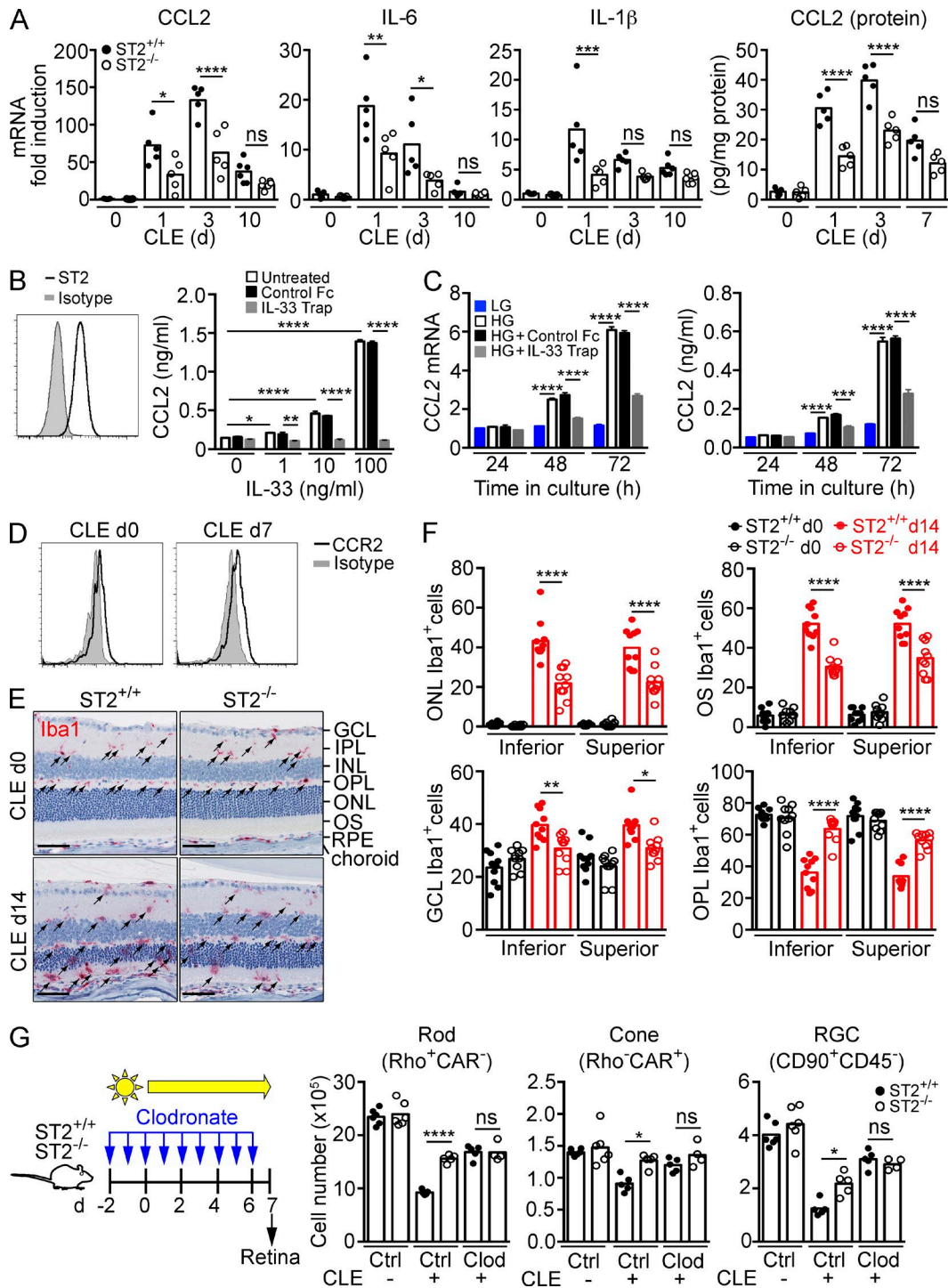
Figure 6. **IL-33 induces chemokine and cytokine expression through autocrine activation of Müller cells.** (A) qPCR analysis of CCL2, IL-6, and IL-1β expression in the retina of ST2+/+ and ST2−/− mice after CLE (n = 5–6/group). Gene expression in d0 ST2+/+ mice was set as 1. CCL2 protein expression in the retina was measured by ELISA. (B) IL-33 induces CCL2 secretion from rMC-1 cells. ST2 expression on the surface of rMC-1 cells was detected by flow cytometry. CCL2 levels in 24-h culture supernatants were measured by ELISA. Data shown are means ± SEM of triplicate wells. (C) Autocrine induction of CCL2 from rMC-1 cells is blocked with IL-33 TRAP. rMC-1 cells were cultured in HG-containing medium in the presence of IL-33 TRAP or a control protein for up to 72 h. CCL2 expression and secretion were measured by qPCR and ELISA, respectively. Data shown are means ± SEM of triplicate experiments. (D) CCR2 expression on retinal CD45^lo^CD11b+ myeloid cells before (d0) and after CLE (d7) was analyzed by flow cytometry. (E and F) Immunohistochemistry analysis of Iba1+ cells in the retina of ST2+/+ and ST2−/− mice. Iba1+ cells (arrows) in the ONL, OS, GCL, and OPL of the entire superior and inferior retina before (d0)

clodronate treatment, indicating that mononuclear phagocytes are required for IL-33/ST2-induced photoreceptor loss when RPE is disrupted.

DISCUSSION

The recently discovered cytokine IL-33 is now well known for its regulation of allergic responses in mucosal tissues (Oliphant et al., 2011; Kearley et al., 2015). However, its role in neuronal tissue is not well understood. This study for the first time shows increased expression of IL-33 in AMD and further demonstrates a role for glia-derived IL-33 in the accumulation of myeloid cells in the outer retina, loss of photoreceptors, and functional impairment of the retina in preclinical models of retina stress.

IL-33 can be released from Müller cells after retina stress to recruit myeloid cells

In the normal rodent neural retina, IL-33 is primarily expressed in Müller cells. Müller cells are important in maintaining laminar structure, metabolic homeostasis, neuronal survival, and retinal regeneration (Bringmann et al., 2006). In response to injury, Müller cells participate in reactive gliosis that could be important for repair of the injured retina but could also have detrimental effects on photoreceptors (Bringmann et al., 2009). We have now demonstrated that IL-33 can be released from Müller cells in vitro and in vivo and that it can act in an autocrine fashion to induce release of inflammatory cytokines and chemokines. The processed C-terminal IL-33 p19 subunit can be released from activated Müller cells in culture and is the only detectable IL-33 protein in the vitreous. Based on our results, we hypothesize that IL-33 undergoes proteolytic cleavage in the nucleus upon Müller cell activation and that this is followed by release of the C-terminal cytokine fold from the nucleus into the extracellular environment. The proteases responsible for processing of IL-33 and the mechanism by which IL-33 is released from Müller cells are unknown and the subject of ongoing studies.

Müller cells are a source of CCL2 after retinal detachment (Nakazawa et al., 2007) and bright light exposure (Rutar et al., 2011, 2012). We now demonstrate that, under conditions of retinal stress and injury, IL-33 contributes to increased expression of CCL2 and the accumulation of CCR2$^+$ myeloid cells in the photoreceptor layer of the retina. ST2 deficiency did not protect the retina in mice depleted of circulating monocytes and macrophages, strongly suggesting that myeloid cell recruitment is required for the pathogenic effect of IL-33–mediated signaling.

Context–dependent protective versus pathogenic role of IL-33

IL-33 may trigger either a protective or destructive response, depending on the location and the nature of the insult. In experimental autoimmune uveitis (EAU), a T cell–driven immune response directed to a retina-specific antigen, IL-33, attenuates disease severity (Barbour et al., 2014). The protective role of IL-33 in EAU was associated with IL-33–mediated skewing of peripheral immune cells toward a protective type 2 immune response. The regulation of systemic type 2 immune responses by IL-33 appears to differ from the regulation of myeloid-driven responses by IL-33 released locally in nervous tissues. In models of acute traumatic CNS injury, glia-derived IL-33 promotes myeloid cell infiltration and improves recovery of affected CNS tissue (Gadani et al., 2015). In a model of *Toxoplasma gondii*–induced encephalitis, IL-33–mediated recruitment of immune cells to the injured CNS serves to limit infection (Jones et al., 2010). Similar to these studies, we demonstrate that local release of IL-33 triggers an inflammatory response characterized by recruitment of monocytes to the injured neuronal tissue. In the retina, these myeloid cells contribute to photoreceptor loss, either directly through phagocytosis of outer segments or indirectly through release of inflammatory mediators (Combadière et al., 2007). The positive association of IL-33 with AMD lesions and the impact of IL-33 on photoreceptor and RGC loss, indicates a pathogenic rather than protective role of IL-33 in both human and rodent retina, in accordance with a previously described pro-inflammatory role of IL-33 in RPE cells (Liu et al., 2012) and a pathogenic role of myeloid cells in the light-stressed retina (Rutar et al., 2011, 2012). Neutralizing IL-33 to reduce myeloid cell accumulation could prevent irreversible loss of photoreceptor cones and rods critical for maintaining vision.

MATERIALS AND METHODS

Mice. ST2 knock-out (ST2$^{-/-}$) BALB/c mice (backcrossed for eight generations) were provided by A. McKenzie (MRC Laboratory of Molecular Biology, Cambridge, London, UK; Townsend et al., 2000). ST2$^{-/-}$ mice were backcrossed to the C57BL/6 background for 10 generations to generate ST2$^{-/-}$ C57BL/6 mice. IL33$^{tm1/+}$ and IL33$^{tm2/tm2}$ BALB/c mice were obtained from A. Iglesias (F. Hoffmann–La Roche Ltd., Basel, Switzerland; Bessa et al., 2014). As a result of significant morbidity and mortality of IL33$^{tm1/+}$ mice, IL33$^{tm1/+}$ mice were crossed with ST2$^{-/-}$ BALB/c mice and maintained on ST2$^{-/-}$ background. IL33$^{tm1/tm1}$ST2$^{+/-}$ mice were generated by breeding female IL33$^{tm1/+}$ST2$^{-/-}$ mice with male

and after CLE (d14) were quantified. Each data point represents an individual mouse (*n* = 10/genotype). Bars, 50 µm. (G) Effect of monocyte depletion on photoreceptor survival in ST2$^{+/+}$ and ST2$^{-/-}$ mice exposed to light. ST2$^{+/+}$ and ST2$^{-/-}$ mice were treated intravenously with clodronate-liposomes (Clod) or control liposomes (Ctrl) daily starting 2 d before CLE as shown in the diagram. Retinal cells were quantified by flow cytometry 7 d after CLE. *n* = 4–6/group. *, P < 0.05; **, P < 0.01; ***, P < 0.001; ****, P < 0.0001; ns, nonsignificant; one-way (A, F, and G) or two-way (B and C) ANOVA with Tukey's post-tests. Data are representative of at least two independent experiments with similar results.
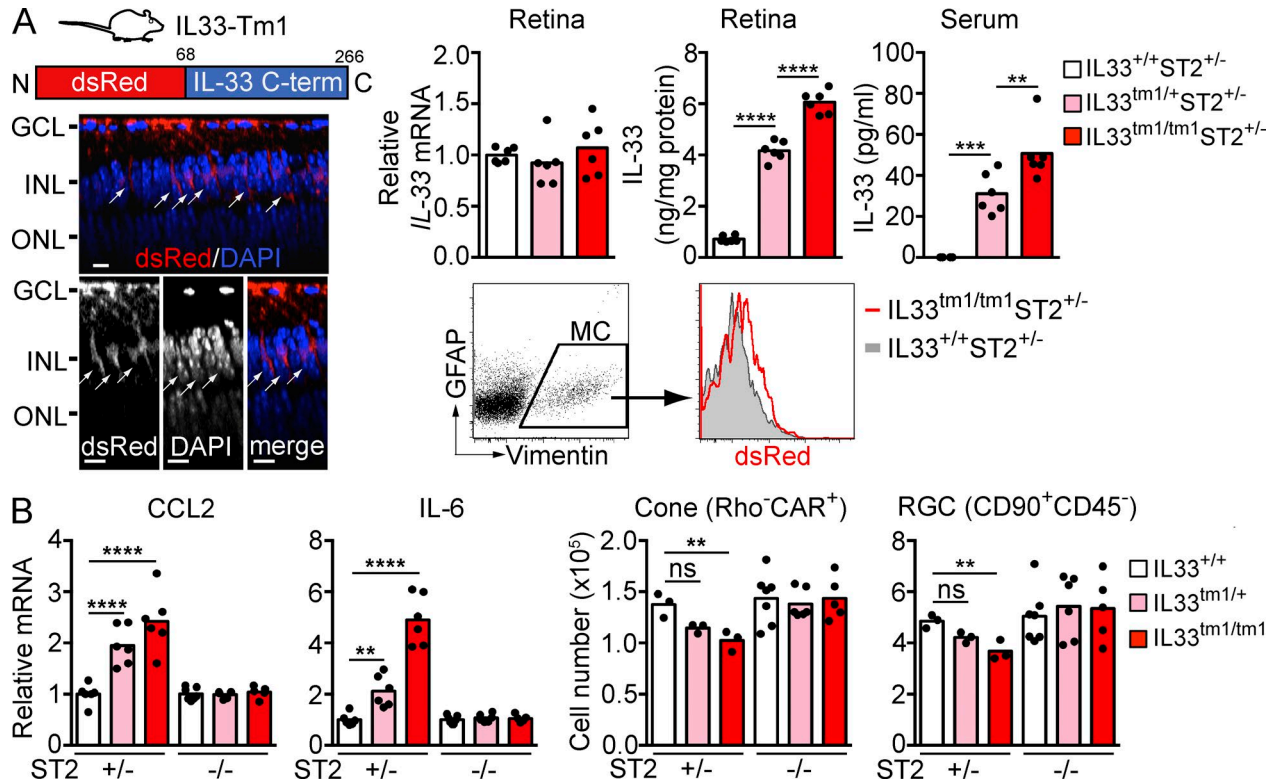
Figure 7. **IL-33 lacking the N-terminus induces ST2–dependent cytokine and chemokine expression and retinal cell loss.** (A) IL33[tm1/tm1] mice lacking the N-terminal nuclear localization sequence and chromatin binding domain (shown in diagram) but retaining the C-terminal cytokine domain show localization of dsRed-IL-33 C-term in cytoplasm of Müller cells. Images shown are Z-section views of confocal images of an IL33[tm1/tm1] retina flat-mount. Arrows, IL-33^{+} Müller cells. Bars, 5 μm. Expression of dsRed-IL-33 C-term in Müller cells was verified by flow cytometry. IL-33 mRNA in the retinas of IL33^{+/+}, IL33[tm1/+], and IL33[tm1/tm1] mice was analyzed by qPCR. IL-33 protein levels in the retina and serum were measured by ELISA. (B) ST2-dependent increases of CCL2 and IL-6 expression and loss of cones and RGC in IL33[tm1/tm1] mice. Retinas from IL33^{+/+}, IL33[tm1/+], and IL33[tm1/tm1] mice bred on ST2^{+/−} or ST2^{−/−} background were analyzed by qPCR and flow cytometry. Each data point represents an individual mouse (n = 3–7/genotype). **, P < 0.01; ***, P < 0.001; ****, P < 0.0001; ns, nonsignificant; one-way ANOVA with Tukey's post-tests. Data are representative of two independent experiments with similar results.

IL33[tm1/+]ST2^{+/+} mice. IL-1R1^{−/−} (Il1r1[tm1Imx]), IL-18R1^{−/−} (Il18r1[tm1Aki]), and IL-18^{−/−} (Il18[tm1Aki]) C57BL/6 mice were purchased from The Jackson Laboratory. IL-1R1^{−/−} and IL-18R1^{−/−} mice were backcrossed to the BALB/c background by speed congenics to generate IL-1R1^{−/−} and IL-18R1^{−/−} BALB/c mice (nine generations), respectively. Sprague-Dawley rats were purchased from Charles River Lab. All animals were housed in pathogen-free animal facility at Genentech with 12/12 h of light/dark cycle, and littermates were used as controls in all experiments. Animal experiments were conducted in accordance with protocols approved by the Genentech Institutional Animal Care and Use Committee and with the ARVO Statement for the Use of Animals in Ophthalmical and Vision Research.

Recombinant proteins. Recombinant mouse IL-33 (aa 109–266) was purchased from R&D Systems. Recombinant rat IL-33 (aa 109–264) was generated by subcloning of a rat cDNA fragment encoding aa 109–264 of IL-33 into a pET28 vector (Novagen). The protein was expressed in

Escherichia coli and purified by Ni-NTA chromatography followed by gel filtration. Recombinant sST2 was generated by subcloning of mouse-soluble ST2 (aa 1–337) in a pRK5 expression vector with 8xHis tag at the C terminus. The fusion protein expressed in CHO cells was purified by Ni-NTA chromatography, followed by Superdex 200 gel filtration. The neutralizing activity of sST2 was verified by blockade of cytokine production from IL-33-stimulated BM-derived mast cell. Recombinant IL-33 TRAP in which the extracellular domain (ECD) of ST2 heterodimerizes with the ECD of IL1RAcP was generated by knob-in-hole technology (Merchant et al., 1998). In brief, a pRK5 expression vector encoding the ECD of mouse ST2 (aa 26–328) with a C-terminal mIgG2a Fc fragment containing knob mutations was cotransfected into CHO cells with a pRK5 expression vector encoding the ECD of mouse IL1RAcP (aa 21–350) with a C-terminal mIgG2a Fc fragment containing "hole" mutations. The fusion protein was purified by MabSURE SELECT column (GE Healthcare) and Superdex 200 gel filtration.
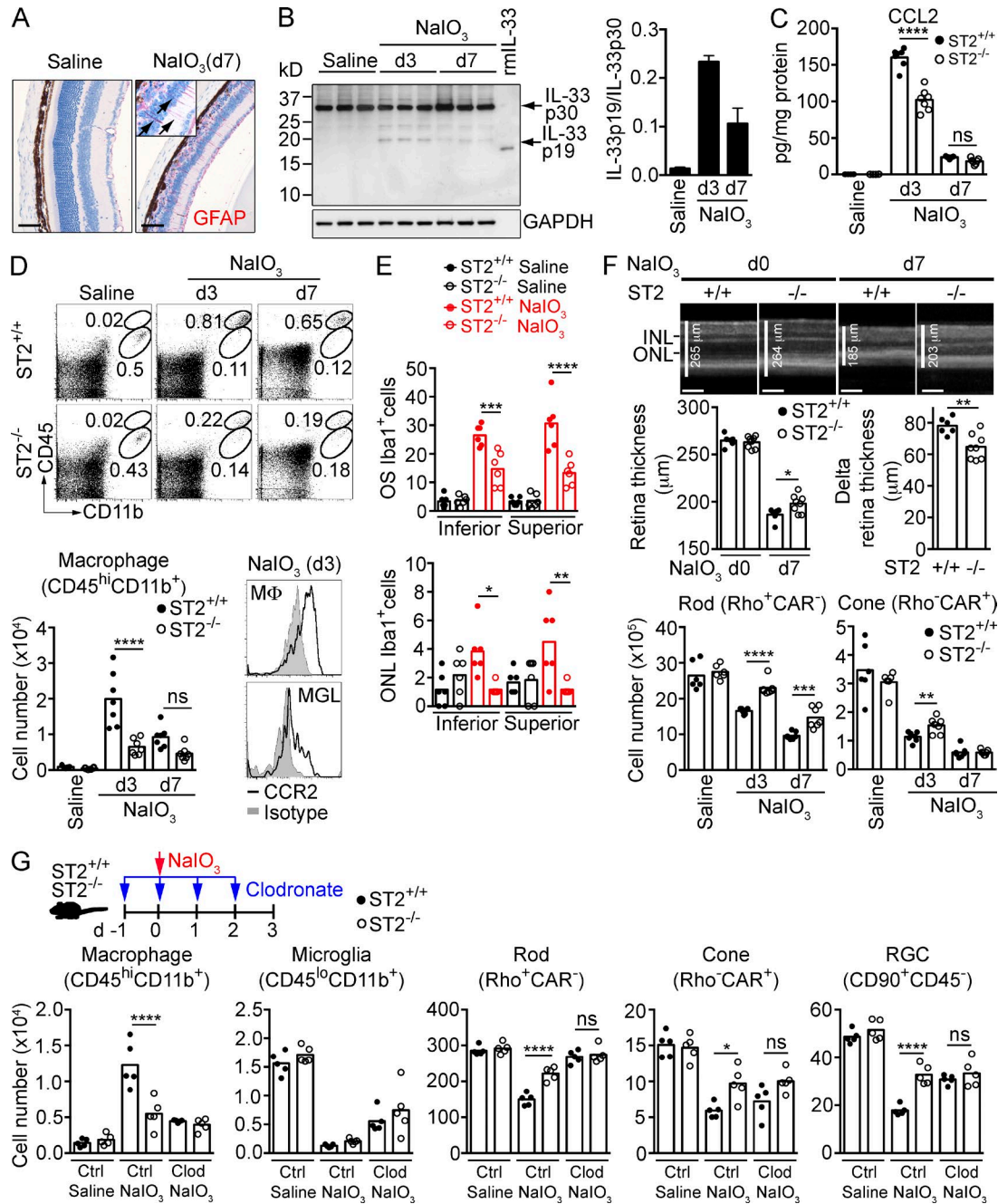
Figure 8. **Mononuclear phagocytes are required for IL-33/ST2-induced photoreceptor cell loss in a model of RPE cell loss.** (A) GFAP expression (red) in Müller cells (arrows) of mice treated with saline or NaIO$_3$. Bar, 50 µm. (B) IL-33 processing in the retina of mice treated with saline or NaIO$_3$ was analyzed by Western blotting. The ratio of IL-33 p19 versus IL-33 p30 in the retina was quantitated with Image J software. (C) CCL2 expression in the retina of ST2$^{+/+}$ and ST2$^{-/-}$ mice treated with saline or NaIO$_3$ was measured by ELISA. n = 6–7/group. (D) Macrophage infiltration in the retina in NaIO$_3$-treated ST2$^{+/+}$ and ST2$^{-/-}$ mice. Macrophages (CD45^{hi}CD11b$^+$) in the retina were quantified by flow cytometry. Retina macrophages express higher level of CCR2 compared with microglia (CD45^{lo}CD11b$^+$). n = 6–7/group. MΦ, macrophage; MGL, microglia. (E) Immunohistochemistry analysis of Iba1$^+$ cells in the retina of NaIO$_3$-treated ST2$^{+/+}$ and ST2$^{-/-}$ mice. Iba1$^+$ cells in the OS and ONL of the entire superior and inferior retina in saline- or NaIO$_3$-treated mice (d3) were quantified. n = 6/group. (F) Protection of photoreceptors in NaIO$_3$-treated ST2$^{-/-}$ mice. (top) Retina thickness of ST2$^{+/+}$ and ST2$^{-/-}$ mice before (d0) and after NaIO$_3$ treatment (d7) was measured by OCT. Representative cross-sectional OCT images are shown. Delta retina thickness was calculated by subtracting the retina thickness of d0 by that of d7 for an individual mouse. Bars, 100 µm. (bottom) Rods and cones of ST2$^{+/+}$ and ST2$^{-/-}$ mice treated with saline or NaIO$_3$ (d3 and d7) were quantified by flow cytometry. Each data point represents an individual mouse (n = 6–8/group). (G) Effect of monocyte depletion on photoreceptor survival in ST2$^{+/+}$ and ST2$^{-/-}$ mice treated with NaIO$_3$. ST2$^{+/+}$ and ST2$^{-/-}$ mice were treated intravenously with clodronate-liposomes (Clod) or control liposomes (Ctrl) daily starting 1 d before NaIO$_3$ treatment as shown in the diagram. Retinal cells were quantified by flow cytometry 3 d after saline

CLE. Male BALB/c mice aged 8–12 wk or Sprague-Dawley rats aged 6–8 wk were kept in normal housing with light intensity of <100 lux (used for baseline, d0). For light exposure, animals were housed singly in slightly modified normal cages covered with only a flat wire rack with no filter lid. To avoid disruption of light entering the cages, food pellets were placed on the bottom of cages and water was provided through a water bottle attached to the side of the cages. Retinal degeneration was induced by placing the cages on the shelves of a Metro rack outfitted with 48-in fluorescent cool white lights above each shelf. The rack was also enclosed in hanging white panels to reflect light evenly back to shelves. Shelf height was adjusted in relation to light source so that light intensity on each shelf was ∼1,200 lux as measured by a light meter. Cages were rotated within each shelf and between shelves during CLE to ensure equal light exposure. Animals were exposed to light for various days, as indicated in Figs. 3, 4, 5 and 6.

RPE damage–induced retinal degeneration. Male C57BL/6 mice aged 6–8 wk were i.v. injected with 20 mg/kg body weight of $NaIO_3$ (Sigma-Aldrich) or vehicle (saline). Retinas were evaluated 3 or 7 d later.

SD–OCT. Retina thickness was measured by SD-OCT using the Spectralis HRA+OCT system (Heidelberg Engineering). To adjust for rodent optics, the system was modified according to the manufacturer's recommendations with a 55 degree wide-field lens placed in front of the camera. Mice were anesthetized by i.p. injection of ketamine (70–80 mg/kg body weight) and xylazine (15 mg/kg body weight). Pupils were dilated with drops of Tropicamide Ophthalmical Solution USP 1% (Bausch & Lomb). Artificial tear was applied bilaterally to prevent corneal dehydration during procedure. Horizontal volume scans through the region dorsal-temporal from the optic nerve (superior quadrant) were used to evaluate the retinal thickness. Total retinal thickness was defined as the width from the inner limiting membrane (ILM) to the RPE/choroid layer on the cross-sectional images, and was measured using custom automated image segmentation routines in MATLAB (MathWorks).

ERG. ERG recordings were performed with the Espion2 electrophysiology system (Diagnosys). Mice were dark-adapted overnight before ERG recording, and all procedures were performed under dim red light. Mice were anesthetized and their pupils were dilated as described in the previous section. Body temperature was maintained using a homeothermic plate and held at 37°C. A reference electrode was inserted s.c. through the forehead and a ground electrode was inserted

s.c. in the lumbar region. A gold–ring electrode (mouse electrode 1.5 mm ø 3.2 mm; LKC Technologies) was placed on the corneal surface of each eye. A drop of Goniovisc Hypermellose Ophthalmical Demulcent Solution 2.5% (HUB Pharmaceuticals) was applied on the cornea to establish optimal electrical contact and to maintain corneal moisture. Mice were placed in a ColorDome light stimulator, and eyes were stimulated with white light of different intensity (0.05, 1, and 25 cd/s/m^2). Maximum rod recovery was obtained by introducing an interstimulus interval ranging from 15 s (lowest stimulus intensity) to 1 min (highest stimulus intensity). Signals were bandpass-filtered at 0.15–1,000 Hz and sampled at 2 kHz. After ERG, ophthalmical ointment was topically applied on the cornea to prevent desiccation. Data were analyzed using custom MATLAB software (MathWorks) with a–wave amplitude measured from the baseline to the trough and b-wave amplitude from the trough to the peak. Responses to 3–5 flashes of light stimulation were averaged.

Clodronate depletion of monocytes/macrophages. To deplete monocytes/macrophages, a dose of 1 mg in 200 µl volume of liposome-encapsulated clodronate (Encapsula Nano Sciences) was administered i.v. daily starting 2 or 1 d before CLE or $NaIO_3$ treatment, respectively. Control mice received the same volume of control liposomes. To monitor systemic monocyte depletion, blood was collected by cardiac puncture under anesthesia with isoflurane. Erythrocytes were removed with ACK lysing buffer (Life Technologies). Cells were resuspended in FACS buffer, Fc blocked, and stained with APC-conjugated anti-CD115 (clone AFS98; eBioscience), FITC-conjugated anti-Ly6C (clone AL-21; BD), and PE-Cy7–conjugated anti-CD11b, and then analyzed by flow cytometry.

Subretinal injection of AAV vectors. The AAV2/5 vector containing mouse sST2 (aa 1–337)-8xHis under the control of the ubiquitous CAG promoter was custom-made by Vector Biosystems. Viral activity was verified by infection of HEK293 cells with multiplicity of infection (MOI) of 10^5 genome copies (GC)/cell. Culture supernatant was harvested 6 d after infection and analyzed for sST2 secretion by ELISA (R&D Systems) and Western blotting using the goat anti–mouse ST2 Ab (R&D Systems). Infection with an AAV empty vector was used as a negative control. For subretinal injection of AAV, BALB/c mice were anesthetized with ketamine/xylazine and pupils were dilated as described in ERG. Under a dissecting microscope, a small incision was made with a 30-gauge needle in the sclera near the junction with the cornea. 1 µl of AAV suspension containing 10^{12} GC/ml was injected into the subretinal space of the right eye through the incision

or $NaIO_3$ treatment. Each data point represents an individual mouse (n = 5/group). *, P < 0.05; **, P < 0.01; ***, P < 0.001; ****, P < 0.0001; ns, nonsignificant; one-way ANOVA with Tukey's post-tests (C, D, E, and G) or unpaired two-tailed Student's t tests (F). Data are representative of at least two independent experiments with similar results.

using a blunt 33-gauge Hamilton needle and an autoinjection device. After injection, a triple antibiotic (Neomycin, Polymyxin B, and Bacitracin) ophthalmical ointment was applied topically to prevent infection and drying of the eye before recovery from anesthesia. 3 wk after infection, sST2 expression in the retina and RPE/choroid was analyzed by ELISA and Western blotting.

Vitreous and retina tissue collection. Rats were euthanized by CO_2 asphyxiation and enucleated. After removal of the cornea, the anterior chamber fluid was absorbed with a Sugi wedge-shaped absorbent swab (Kettenbach Medical). The lens with the vitreous humor attached was carefully pulled out from the posterior chamber using an angled microsurgical forceps. The lens-vitreous humor was placed into a filtered centrifugation tube (Costar) containing 20 µl of protease inhibitor cocktail (Roche) dissolved in PBS and centrifuged at 14,000 g for 5 min at 4°C. The vitreous was collected from the lower chamber. The retina was separated from the sclera and RPE/choroid, rinsed in PBS, and either dissociated for FACS analysis or homogenized in the cell lysis buffer (Cell Signaling Technology) using a tissue homogenizer (IKA) for ELISA and Western blotting. The retina and RPE/choroid homogenate was centrifuged at 14, 000 g for 10 min at 4°C, and the supernatant was collected.

Flow cytometry. Retina was isolated as described in the previous section and digested with Earle's balanced salt solution (EBSS) containing 20 IU/ml papain and 200 IU/ml DNase (Worthington Biochemicals) for 30 min at 37°C. Tissue was dissociated by gentle pipetting. Papain digestion was terminated by resuspending the retinal cells in EBSS containing the ovomucoid protease inhibitor (Worthington Biochemicals). Total retinal cells were quantified by mixing an aliquot of single-cell suspension 1:1 with a standard concentration of 6 µm Fluoresbrite YG microspheres (Polysciences), followed by counting on an LSRFortessa flow cytometer (BD). Live cells were gated on propidium iodide–negative (PI^-) cells. Primary retinal cells were resuspended in FACS buffer (PBS containing 0.5% bovine serum albumin and 2 mM EDTA, pH 8.0) and incubated with anti-CD16/CD32 (BD) for 30 min to block any nonspecific binding to Fc receptors. Retinal cells were stained with PE-Cy7–conjugated anti-CD11b (clone M1/70; BD), APC-conjugated anti-CD90.2 (clone 53–2.1; BD), Alexa Fluor 700–conjugated anti-CD45 (clone 30-F11; BioLegend), FITC-conjugated anti-ST2 (clone DJ8; MD Bioproducts), and PE-conjugated anti-CCR2 (R&D Systems). To detect intracellular markers, the following fluorophore-conjugated Abs were generated using Ab conjugation kits (Abcam) according to the manufacturer's instructions: PE-Cy7–conjugated antirhodopsin (Rho; clone 1D4; EMD Millipore), PE-conjugated anti-cone arrestin (CAR; EMD Millipore), and PerCP-Cy5.5–conjugated anti-GFAP (clone GA5; Thermo Fisher Scientific). Alexa Fluor 647–conjugated anti-vimentin (clone D21H3) was purchased from Cell Sig-

naling Technology. Cells were stained with violet fixable viability dye (Life Technologies), fixed, and permeabilized with IntraPrep permeabilization reagent (Beckman Coulter) according to manufacturer's instructions. Cells were then stained with the Ab cocktail for 30 min, washed, and analyzed on the LSRFortessa flow cytometer. All data were acquired with BD FACSDiva software and analyzed with FlowJo software (GraphPad). Total numbers of rods (Rho^+CAR^-), cones (Rho^-CAR^+), ganglion cells ($CD90^+CD45^-$), microglia ($CD45^{lo}CD11b^+$), and macrophages ($CD45^{hi}CD11b^+$) were calculated by multiplying the percentage of each cell type with total live retinal cells.

rMC-1 stimulation. rMC-1 cells (Kerafast) were maintained in low glucose (5.5 mM) containing DMEM (LG-DMEM) with 10% heat-inactivated FBS, 100 U/ml penicillin, and 100 µg/ml streptomycin. For high glucose stimulation, 5×10^5 cells were cultured in 2 ml of LG-DMEM with 2% FBS in 6-well plate at 37°C overnight. The medium was replaced by either LG-DMEM or high glucose (25 mM) containing DMEM (HG-DMEM) with 2% FBS and cultured for up to 72 h. Cell viability was determined by staining the cells with Annexin V and PI using the FITC Annexin V Apoptosis Detection kit (BD) according to the manufacturer's instructions. Culture supernatant was harvested and IL-33 expression was analyzed by ELISA and Western blotting. For IL-33 stimulation of rMC-1 cells, 2×10^5 cells were cultured in 1 ml of LG-DMEM with 10% FBS in a 12-well plate and stimulated with rat IL-33 (1, 10, and 100 ng/ml) for 24 h. ST2-dependent activity of IL-33 on rMC-1 cells was determined by stimulating the cells with IL-33 in the presence of 10 µg/ml IL-33 TRAP or a control Fc protein. CCL2 levels in the culture supernatant were measured by ELISA. To determine autocrine activity of IL-33 in rMC-1 cells, cells were cultured in (HG-DMEM) with 2% FBS in the presence of 10 µg/ml IL-33 TRAP or a control Fc protein for various time as indicated in Fig. 6 C. RNA and culture supernatant were collected for CCL2 expression by qPCR and ELISA, respectively.

ELISA. IL-33 concentrations in the vitreous, retina lysate, serum, and rMC-1 culture supernatant were measured using the mouse/rat IL-33 Quantikine ELISA kit (R&D Systems). CCL2, IL-1α, IL-1β, and ST2 were quantified with Quantikine ELISA kits. IL-18 was measured with mouse IL-18 ELISA kit (MBL International). Cytokine concentrations in the retina lysate were normalized to total protein content measured by BCA assay (Thermo Fisher Scientific). To assess IL-33 levels in the vitreous of AMD patients, patients diagnosed with AMD (one male and five females, age 68–91, median age 79), macular pucker (three males and nine females, age 56–79, median age 72), and macular hole (5 males and 16 females, age 46–75, median age 65) were followed and operated by a single vitreoretinal surgeon (Midwest Eye Institute) with approval from Western Institutional Review Board (WIRB) and written patient informed consent. Transcon-

junctival pars plana vitrectomy was performed under local anesthesia using a 25-gauge cannula (Alcon). IL-33 levels in the vitreous were measured using the human IL-33 Quanti-kine ELISA kit (R&D Systems).

RT–PCR. Total RNA was isolated from retina and rMC-1 cells using the RNeasy Plus Mini kit (QIAGEN). First strand cDNA was synthesized using the High-Capacity cDNA Reverse Transcription kit (Applied Biosystems). Quantitative PCR (qPCR) of IL-33, CCL2, ST2L, sST2, IL-6, IL-1α, IL-1β, and IL-18 was performed using the TaqMan Gene Expression Assay with verified primer and probe sets (Applied Biosystems) and the levels were normalized by expression of 18s rRNA (mouse) or β-actin (rat). To examine potential alternative splice variants of IL-33 in rMC-1 cells and rat retina, we performed RT-PCR using PCR primers spanning the 5′UTR (exon 1) and the stop codon (exon 9) of the full-length IL-33 mRNA as follows: 5′-TTAAGACCAGCTA TCTCCCATCA-3′ (Forward) and 5′-ACGTTACATCTTA GAGAGCTTAAACA-3′ (Reverse). PCR was performed using the Expand High Fidelity PCR System (Roche) according to the manufacturer's instructions. The resulting PCR products were analyzed by electrophoresis on 1% agarose gel.

Western blotting. Vitreous, retina lysates, RPE/choroid lysates, or rMC-1 culture supernatants were separated by electrophoresis on Novex SDS-Tris–Glycine polyacrylamide gels (Life Technologies) and transferred to nitrocellulose membranes using the iBlot system (Invitrogen). After blocking, the membranes were probed with goat anti–mouse C-terminal IL-33 (AF3626, R&D Systems) that cross-reacts to rat IL-33, or goat anti-mouse ST2 (R&D Systems), or rabbit anti-GAP DH (Cell Signaling Technology), followed by probing with appropriate HRP-conjugated secondary Abs (Jackson ImmunoResearch Laboratories). Blots were processed using ECL Plus Western blot detection reagents (GE Healthcare). Nuclear and cytoplasmic fractions of rMC-1 cells were separated using the NE-PER Nuclear and Cytoplasmic Extraction reagent (Thermo Fisher Scientific) according to the manufacturer's instructions. Protein concentration was quantitated by the BCA protein assay. Equal amounts of protein were analyzed for IL-33 expression by Western blotting. Subcellular fractionation of nucleus and cytoplasm was verified by probing the blot with mouse anti–HDAC2 and anti-HSP90 (EMD Millipore), respectively.

Microarray analysis. Total RNA was converted to double-stranded cDNA and then to Cy-dye labeled cRNA using an Agilent Fluorescent Linear Amplification kit. Cy-dye-labeled cRNA was fragmented and hybridized to the Agilent's whole mouse genome array as described in Agilent's In Situ Hybridization Plus kit. All samples were labeled with Cy5 dye and hybridized against Cy3 dye–labeled universal mouse reference. After hybridization, the arrays were washed, dried and scanned on Agilent's DNA microarray scanner. Array im-

aging data were analyzed using Agilent's Feature Extraction software 8.5. Raw feature extracted data were processed as previously described (Vander Lugt et al., 2014). Microarray data were filtered to include only a single probe per gene, selecting the probe with the highest variance when multiple probes were present for a given gene (Bourgon et al., 2010). Differential expression analysis was performed using the limma software package (Smyth, 2004). To identify genes differentially regulated in the ST2$^{-/-}$ mice, we first identified probes up-regulated by CLE in ST2$^{+/+}$ mice, selecting probes that showed >1.5-fold change at a Benjamini-Hochberg (Hochberg and Benjamini, 1990) adjusted p-value of <0.01. These probes were further filtered to those that showed >1.25-fold difference at a Benjamini-Hochberg adjusted p-value of <0.05 between ST2$^{+/+}$ and ST2$^{-/-}$ mice. The microarray data are deposited at NCBI GEO database under accession no. GSE74695.

Gene ontology analysis. Genes identified as differentially expressed were subjected to gene ontology analysis using the GOstats R package (Falcon and Gentleman, 2007). We used the set of genes differentially regulated by ST2$^{+/+}$ and ST2$^{-/-}$ mice as our test set, and the set of genes differentially regulated by CLE as our universe of genes to consider. We restricted our search to the biological process ontology, using a conditional test of significance. Gene ontology terms that showed significant enrichment at a nominal (unadjusted) p-value of 0.01 were selected.

RNA sequencing. For RNA sequencing analysis of human retina, postmortem healthy donor eyes with no history of ocular diseases were acquired from the Lions Eye Institute for Transplant and Research in Tampa, Florida. The human donor eyes were obtained and used in accordance with the guidelines of the Declaration of Helsinki for research involving the use of human tissue and with written donor informed consent. Donor eyes were enucleated 4 h or less postmortem and preserved in RNAlater immediately after collection. The macula is fully contained within the boundaries of superior and inferior temporal vascular arcades and is easily visualized. After the macula was dissected out from the peripheral fundus using dissecting scissors, the macular retina was separated from the RPE and choroid underneath the retina. Total RNA was isolated from the retina using RNeasy Mini kit (QIAGEN). RNA concentration was determined using a NanoDrop 8000 Spectrophotometer. Samples preserved in RNAlater usually yield high quality as assessed with an Agilent 2100 Bioanalyzer (Agilent Technologies). RNA-seq libraries were prepared using the TruSeq RNA Sample Preparation kit (Illumina) according to the manufacturer's instructions and then sequenced by an Illumina HiSeq 2000 system (Illumina). Sequencing data analysis was performed as previously described (Durinck et al., 2015). Sequencing reads were mapped to the reference human genome (GRCh37), using the GSNAP short read aligner (Wu and Nacu, 2010).

Expression was measured in reads per kilobase per million total reads (RPKM) by normalizing the number of reads aligning to coding sequence in a given gene to the total length of the coding sequence and the total number of reads.

Histology and immunohistochemistry. For morphometric analysis of the outer nuclear layer (ONL) thickness, mouse eyes were fixed in Davidson's fixative (Electron Microscopy Sciences) for 24 h. Paraffin-embedded 4 µm sections covering the entire retina, including the optic nerve, were cut along the vertical meridian of the globe and stained with hematoxylin and eosin (H&E). After mounting of the sections, slides were scanned using an Olympus Nanozoomer 2.0 HT digital slide scanner (Hamamatsu) running NDP Scan software with an Olympus Uplan SApo 0.75 NA 20x objective lens. Images were analyzed using custom automated image segmentation routines in Matlab (MathWorks). Only sections cut through optic nerves were analyzed. The ONL thickness was measured at a distance of 0.1, 0.2, 0.3, 0.4, 0.6, 0.8 and 1.0 mm starting from either side of the optic nerve head. IL33$^{tm2/tm2}$ and IL33$^{tm1/tm1}$ eyes were fixed in 4% paraformaldehyde for 2 h and rinsed in PBS. Retina tissues were dissected intact from the globe and stained with 1 µg/ml DAPI (Invitrogen) in PBST buffer (1x PBS, 0.5% Tween 20) for 2 h, followed by washing five times in PBST buffer and rinsing in PBS. The retina was flat-mounted and imaged with a Nikon A1R confocal microscope using a 40× objective lens. Images in Fig. 3 F and Fig. 7 A were optimized by making minor adjustments to brightness and contrast using Photoshop (Adobe). For IL-33 and vimentin co-staining, rat eyes were fixed in Davidson's fixative for 24 h, immersed in 70% ethanol, and processed for paraffin embedding and sectioning. IHC staining of sections was performed on a Dako Autostainer platform (Dako). After rehydration, sections were treated in Dako Target Retrieval Solution (Dako). Sections were incubated with 5 µg/ml of a mouse mAb to IL-33 (clone Nessy 1; Enzo Life Sciences) and 0.18 µg/ml rabbit mAb to vimentin (Cell Signaling Technologies) or negative control Abs in blocking buffer for 1 h. After washing, the sections were incubated with PowerVision Poly-HRP anti–mouse IgG and Poly-AP anti–rabbit IgG (Leica Biosystems) for 30 min followed by detection with diaminobenzidine (DAB) and Fast Red/Naphthol Phosphate reagent (ScyTek). After counterstaining with hematoxylin, the sections were imaged with bright field microscopy. IL-33, GFAP, and Iba1 staining of mouse eyes were performed in the same way with a goat polyclonal Ab to IL-33 (AF3626; R&D Systems; 0.1 µg/ml), a rabbit polyclonal Ab to GFAP (DAKO; 1:500) and a rabbit polyclonal Ab to Iba1 (Wako Chemicals; 0.5 µg/ml), respectively. Myeloid cell quantification was performed by manually counting the Iba1$^+$ cells in each retinal layer along the full length of retinal sections cut in the vertical meridian, including the optic disc. TUNEL staining of rat eye sections was performed with the ApoTag Peroxidase In Situ Apoptosis Detection kit (EMD Millipore) according to the manufactur-

er's instructions. For IHC analysis of human eyes, postmortem eyes from seven normal donors (five males and two females) with age range of 67–89 yr and seven AMD patients (two males and five females) with age range of 82–92 yr were obtained from the Lions Eye Institute for Transplant and Research in Tampa, Florida. All eyes were obtained and used in accordance with the guidelines of the Declaration of Helsinki for research involving the use of human tissue and with written donor informed consent. Eyes were fixed in Davidson's fixative for 24 h and immersed in 70% ethanol. An incision was made temporal and medial of the optic nerve to obtain a ~10-mm-thick vertical slice that encompassed the fovea, macula, and peripheral retina. Following paraffin embedding, 4-µm sections that included the fovea were cut along the vertical meridian of the globe and stained with H&E. Fluorescent IHC costaining of IL-33, vimentin, GFAP, Iba1, and PLVAP were performed using the Abs as described above and Genentech mouse mAb to PLVAP, followed by staining with appropriate Fluorescent dye-labeled secondary Abs or Fluorescent dye-TSA (tyramide signal amplification) and counterstaining with DAPI. Slides were scanned in a digital slide scanner as described above. Brightness was slightly adjusted for images in Fig. 1 and Fig. 2 using NDP view 2 software (Hamamatsu) to better visualize the signal, but all images within a panel were similarly modified. IL-33$^+$ and Iba1$^+$ cell quantification were performed by manually counting IL-33$^+$ and Iba1$^+$ cells along a ~500-µm region in the central and peripheral area of control eyes or lesion and non-lesion area of AMD eyes.

Statistical analysis. All data, unless otherwise indicated, were analyzed and graphed using Prism 6 software (GraphPad). Statistical analysis was performed using an unpaired two-tailed Student's *t* test or ANOVA as indicated for comparison between groups. $P < 0.05$ was considered significant.

Online supplemental material. Fig. S1, Table S1, and Table S2 describe microarray analysis of light-injured retina from ST2$^{+/+}$ and ST2$^{-/-}$ mice. Online supplemental material is available at http://www.jem.org/cgi/content/full/jem. 20150894/DC1.

REFERENCES

Alves-Filho, J.C., F. Sônego, F.O. Souto, A. Freitas, W.A. Verri Jr., M. Auxiliadora-Martins, A. Basile-Filho, A.N. McKenzie, D. Xu, F.Q. Cunha, and F.Y. Liew. 2010. Interleukin-33 attenuates sepsis by enhancing neutrophil influx to the site of infection. *Nat. Med.* 16:708–712. http://dx.doi.org/10.1038/nm.2156

Baekkevold, E.S., M. Roussigné, T. Yamanaka, F.E. Johansen, F.L. Jahnsen, F. Amalric, P. Brandtzaeg, M. Erard, G. Haraldsen, and J.P. Girard. 2003. Molecular characterization of NF-HEV, a nuclear factor preferentially expressed in human high endothelial venules. *Am. J. Pathol.* 163:69–79. http://dx.doi.org/10.1016/S0002-9440(10)63631-0

Barbour, M., D. Allan, H. Xu, C. Pei, M. Chen, W. Niedbala, S.Y. Fukada, A.G. Besnard, J.C. Alves-Filho, X. Tong, et al. 2014. IL-33 attenuates the development of experimental autoimmune uveitis. *Eur. J. Immunol.* 44:3320–3329. http://dx.doi.org/10.1002/eji.201444671

Bessa, J., C.A. Meyer, M.C. de Vera Mudry, S. Schlicht, S.H. Smith, A. Iglesias, and J. Cote-Sierra. 2014. Altered subcellular localization of IL-33 leads to non-resolving lethal inflammation. *J. Autoimmun.* 55:33–41. http://dx.doi.org/10.1016/j.jaut.2014.02.012

Bhutto, I., and G. Lutty. 2012. Understanding age-related macular degeneration (AMD): relationships between the photoreceptor/retinal pigment epithelium/Bruch's membrane/choriocapillaris complex. *Mol. Aspects Med.* 33:295–317. http://dx.doi.org/10.1016/j.mam.2012.04.005

Bourgon, R., R. Gentleman, and W. Huber. 2010. Independent filtering increases detection power for high-throughput experiments. *Proc. Natl. Acad. Sci. USA.* 107:9546–9551. http://dx.doi.org/10.1073/pnas.0914005107

Bringmann, A., T. Pannicke, J. Grosche, M. Francke, P. Wiedemann, S.N. Skatchkov, N.N. Osborne, and A. Reichenbach. 2006. Müller cells in the healthy and diseased retina. *Prog. Retin. Eye Res.* 25:397–424. http://dx.doi.org/10.1016/j.preteyeres.2006.05.003

Bringmann, A., I. Iandiev, T. Pannicke, A. Wurm, M. Hollborn, P. Wiedemann, N.N. Osborne, and A. Reichenbach. 2009. Cellular signaling and factors involved in Müller cell gliosis: neuroprotective and detrimental effects. *Prog. Retin. Eye Res.* 28:423–451. http://dx.doi.org/10.1016/j.preteyeres.2009.07.001

Carido, M., Y. Zhu, K. Postel, B. Benkner, P. Cimalla, M.O. Karl, T. Kurth, F. Paquet-Durand, E. Koch, T.A. Münch, et al. 2014. Characterization of a mouse model with complete RPE loss and its use for RPE cell transplantation. *Invest. Ophthalmol. Vis. Sci.* 55:5431–5444. http://dx.doi.org/10.1167/iovs.14-14325

Chovatiya, R., and R. Medzhitov. 2014. Stress, inflammation, and defense of homeostasis. *Mol. Cell.* 54:281–288. http://dx.doi.org/10.1016/j.molcel.2014.03.030

Combadière, C., C. Feumi, W. Raoul, N. Keller, M. Rodéro, A. Pézard, S. Lavalette, M. Houssier, L. Jonet, E. Picard, et al. 2007. CX3CR1-dependent subretinal microglia cell accumulation is associated with cardinal features of age-related macular degeneration. *J. Clin. Invest.* 117:2920–2928. http://dx.doi.org/10.1172/JCI31692

de Jong, P.T. 2006. Age-related macular degeneration. *N. Engl. J. Med.* 355:1474–1485. http://dx.doi.org/10.1056/NEJMra062326

Doyle, S.L., M. Campbell, E. Ozaki, R.G. Salomon, A. Mori, P.F. Kenna, G.J. Farrar, A.S. Kiang, M.M. Humphries, E.C. Lavelle, et al. 2012. NLRP3 has a protective role in age-related macular degeneration through the induction of IL-18 by drusen components. *Nat. Med.* 18:791–798. http://dx.doi.org/10.1038/nm.2717

Doyle, S.L., E. Ozaki, K. Brennan, M.M. Humphries, K. Mulfaul, J. Keaney, P.F. Kenna, A. Maminishkis, A.S. Kiang, S.P. Saunders, et al. 2014. IL-18 attenuates experimental choroidal neovascularization as a potential therapy for wet age-related macular degeneration. *Sci. Transl. Med.* 6:230ra44. http://dx.doi.org/10.1126/scitranslmed.3007616

Durinck, S., E.W. Stawiski, A. Pavía-Jiménez, Z. Modrusan, P. Kapur, B.S. Jaiswal, N. Zhang, V. Toffessi-Tcheuyap, T.T. Nguyen, K.B. Pahuja, et al. 2015. Spectrum of diverse genomic alterations define non-clear cell renal carcinoma subtypes. *Nat. Genet.* 47:13–21. http://dx.doi.org/10.1038/ng.3146

Espinassous, Q., E. Garcia-de-Paco, I. Garcia-Verdugo, M. Synguelakis, S. von Aulock, J.M. Sallenave, A.N. McKenzie, and J. Kanellopoulos. 2009. IL-33 enhances lipopolysaccharide-induced inflammatory cytokine production from mouse macrophages by regulating lipopolysaccharide receptor complex. *J. Immunol.* 183:1446–1455. http://dx.doi.org/10.4049/jimmunol.0803067

Falcon, S., and R. Gentleman. 2007. Using GOstats to test gene lists for GO term association. *Bioinformatics.* 23:257–258. http://dx.doi.org/10.1093/bioinformatics/btl567

Gadani, S.P., J.T. Walsh, I. Smirnov, J. Zheng, and J. Kipnis. 2015. The glia-derived alarmin IL-33 orchestrates the immune response and promotes recovery following CNS injury. *Neuron.* 85:703–709. http://dx.doi.org/10.1016/j.neuron.2015.01.013

Gadina, M., and C.A. Jefferies. 2007. IL-33: A sheep in wolf's clothing?. *Sci. STKE.* 2007:pe31. http://dx.doi.org/10.1126/stke.3902007pe31

Guo, C., A. Otani, A. Oishi, H. Kojima, Y. Makiyama, S. Nakagawa, and N. Yoshimura. 2012. Knockout of ccr2 alleviates photoreceptor cell death in a model of retinitis pigmentosa. *Exp. Eye Res.* 104:39–47. http://dx.doi.org/10.1016/j.exer.2012.08.013

Hochberg, Y., and Y. Benjamini. 1990. More powerful procedures for multiple significance testing. *Stat. Med.* 9:811–818. http://dx.doi.org/10.1002/sim.4780090710

Hu, S.J., B. Calippe, S. Lavalette, C. Roubeix, F. Montassar, M. Housset, O. Levy, C. Delarasse, M. Paques, J.A. Sahel, et al. 2015. Upregulation of P2RX7 in Cx3cr1-deficient mononuclear phagocytes leads to increased interleukin-1β secretion and photoreceptor neurodegeneration. *J. Neurosci.* 35:6987–6996. http://dx.doi.org/10.1523/JNEUROSCI.3955-14.2015

Hueber, A.J., J.C. Alves-Filho, D.L. Asquith, C. Michels, N.L. Millar, J.H. Reilly, G.J. Graham, F.Y. Liew, A.M. Miller, and I.B. McInnes. 2011. IL-33 induces skin inflammation with mast cell and neutrophil activation. *Eur. J. Immunol.* 41:2229–2237. http://dx.doi.org/10.1002/eji.201041360

Jarrett, S.G., and M.E. Boulton. 2012. Consequences of oxidative stress in age-related macular degeneration. *Mol. Aspects Med.* 33:399–417. http://dx.doi.org/10.1016/j.mam.2012.03.009

Jones, L.A., F. Roberts, M.B. Nickdel, F. Brombacher, A.N. McKenzie, F.L. Henriquez, J. Alexander, and C.W. Roberts. 2010. IL-33 receptor (T1/ST2) signalling is necessary to prevent the development of encephalitis in mice infected with *Toxoplasma gondii*. *Eur. J. Immunol.* 40:426–436. http://dx.doi.org/10.1002/eji.200939705

Kearley, J., J.S. Silver, C. Sanden, Z. Liu, A.A. Berlin, N. White, M. Mori, T.H. Pham, C.K. Ward, G.J. Criner, et al. 2015. Cigarette smoke silences innate lymphoid cell function and facilitates an exacerbated type I interleukin-33-dependent response to infection. *Immunity.* 42:566–579. http://dx.doi.org/10.1016/j.immuni.2015.02.011

Kim, J., W. Kim, H.T. Le, U.J. Moon, V.G. Tran, H.J. Kim, S. Jung, Q.T. Nguyen, B.S. Kim, J.B. Jun, et al. 2014. IL-33-induced hematopoietic stem and progenitor cell mobilization depends upon CCR2. *J. Immunol.* 193:3792–3802. http://dx.doi.org/10.4049/jimmunol.1400176

LaVail, M.M., K. Unoki, D. Yasumura, M.T. Matthes, G.D. Yancopoulos, and R.H. Steinberg. 1992. Multiple growth factors, cytokines, and neurotrophins rescue photoreceptors from the damaging effects of constant light. *Proc. Natl. Acad. Sci. USA.* 89:11249–11253. http://dx.doi.org/10.1073/pnas.89.23.11249

Lavalette, S., W. Raoul, M. Houssier, S. Camelo, O. Levy, B. Calippe, L. Jonet, F. Behar-Cohen, S. Chemtob, X. Guillonneau, et al. 2011. Interleukin-1β inhibition prevents choroidal neovascularization and does not exacerbate photoreceptor degeneration. *Am. J. Pathol.* 178:2416–2423. http://dx.doi.org/10.1016/j.ajpath.2011.01.013

Lefrançais, E., S. Roga, V. Gautier, A. Gonzalez-de-Peredo, B. Monsarrat, J.P. Girard, and C. Cayrol. 2012. IL-33 is processed into mature bioactive forms by neutrophil elastase and cathepsin G. *Proc. Natl. Acad. Sci. USA.* 109:1673–1678. http://dx.doi.org/10.1073/pnas.1115884109

Lingel, A., T.M. Weiss, M. Niebuhr, B. Pan, B.A. Appleton, C. Wiesmann, J.F. Bazan, and W.J. Fairbrother. 2009. Structure of IL-33 and its interaction with the ST2 and IL-1RAcP receptors—Insight into heterotrimeric IL-1 signaling complexes. *Structure.* 17:1398–1410. http://dx.doi.org/10.1016/j.str.2009.08.009

Liu, X., M. Hammel, Y. He, J.A. Tainer, U.S. Jeng, L. Zhang, S. Wang, and X. Wang. 2013. Structural insights into the interaction of IL-33 with its receptors. *Proc. Natl. Acad. Sci. USA.* 110:14918–14923. http://dx.doi.org/10.1073/pnas.1308651110

Liu, X.C., X.F. Liu, C.X. Jian, C.J. Li, and S.Z. He. 2012. IL-33 is induced by amyloid-β stimulation and regulates inflammatory cytokine production in retinal pigment epithelium cells. *Inflammation.* 35:776–784. http://dx.doi.org/10.1007/s10753-011-9379-4

Maeda, A., G. Palczewska, M. Golczak, H. Kohno, Z. Dong, T. Maeda, and K. Palczewski. 2014. Two-photon microscopy reveals early rod photoreceptor cell damage in light-exposed mutant mice. *Proc. Natl. Acad. Sci. USA.* 111:E1428–E1437. http://dx.doi.org/10.1073/pnas.1317986111

Merchant, A.M., Z. Zhu, J.Q. Yuan, A. Goddard, C.W. Adams, L.G. Presta, and P. Carter. 1998. An efficient route to human bispecific IgG. *Nat. Biotechnol.* 16:677–681. http://dx.doi.org/10.1038/nbt0798-677

Nakazawa, T., T. Hisatomi, C. Nakazawa, K. Noda, K. Maruyama, H. She, A. Matsubara, S. Miyahara, S. Nakao, Y. Yin, et al. 2007. Monocyte chemoattractant protein 1 mediates retinal detachment-induced photoreceptor apoptosis. *Proc. Natl. Acad. Sci. USA.* 104:2425–2430. http://dx.doi.org/10.1073/pnas.0608167104

Oliphant, C.J., J.L. Barlow, and A.N. McKenzie. 2011. Insights into the initiation of type 2 immune responses. *Immunology.* 134:378–385. http://dx.doi.org/10.1111/j.1365-2567.2011.03499.x

Pichery, M., E. Mirey, P. Mercier, E. Lefrancais, A. Dujardin, N. Ortega, and J.P. Girard. 2012. Endogenous IL-33 is highly expressed in mouse epithelial barrier tissues, lymphoid organs, brain, embryos, and inflamed tissues: in situ analysis using a novel Il-33–LacZ gene trap reporter strain. *J. Immunol.* 188:3488–3495. http://dx.doi.org/10.4049/jimmunol.1101977

Rivera, J.C., N. Sitaras, B. Noueihed, D. Hamel, A. Madaan, T. Zhou, J.C. Honoré, C. Quiniou, J.S. Joyal, P. Hardy, et al. 2013. Microglia and interleukin-1β in ischemic retinopathy elicit microvascular degeneration through neuronal semaphorin-3A. *Arterioscler. Thromb. Vasc. Biol.* 33:1881–1891. http://dx.doi.org/10.1161/ATVBAHA.113.301331

Rutar, M., R. Natoli, K. Valter, and J.M. Provis. 2011. Early focal expression of the chemokine Ccl2 by Müller cells during exposure to damage-inducing bright continuous light. *Invest. Ophthalmol. Vis. Sci.* 52:2379–2388. http://dx.doi.org/10.1167/iovs.10-6010

Rutar, M., R. Natoli, and J.M. Provis. 2012. Small interfering RNA–mediated suppression of Ccl2 in Müller cells attenuates microglial recruitment and photoreceptor death following retinal degeneration. *J. Neuroinflammation.* 9:221. http://dx.doi.org/10.1186/1742-2094-9-221

Rutar, M., R. Natoli, R.X. Chia, K. Valter, and J.M. Provis. 2015. Chemokine-mediated inflammation in the degenerating retina is coordinated by Müller cells, activated microglia, and retinal pigment epithelium. *J. Neuroinflammation.* 12:8. http://dx.doi.org/10.1186/s12974-014-0224-1

Sarthy, V.P., S.J. Brodjian, K. Dutt, B.N. Kennedy, R.P. French, and J.W. Crabb. 1998. Establishment and characterization of a retinal Müller cell line. *Invest. Ophthalmol. Vis. Sci.* 39:212–216.

Schmitz, J., A. Owyang, E. Oldham, Y. Song, E. Murphy, T.K. McClanahan, G. Zurawski, M. Moshrefi, J. Qin, X. Li, et al. 2005. IL-33, an interleukin-1-like cytokine that signals via the IL-1 receptor-related protein ST2 and induces T helper type 2-associated cytokines. *Immunity.* 23:479–490. http://dx.doi.org/10.1016/j.immuni.2005.09.015

Sennlaub, F., C. Auvynet, B. Calippe, S. Lavalette, L. Poupel, S.J. Hu, E. Dominguez, S. Camelo, O. Levy, E. Guyon, et al. 2013. CCR2^{+} monocytes infiltrate atrophic lesions in age-related macular disease and mediate photoreceptor degeneration in experimental subretinal inflammation in Cx3cr1 deficient mice. *EMBO Mol. Med.* 5:1775–1793. http://dx.doi.org/10.1002/emmm.201302692

Smyth, G.K. 2004. Linear models and empirical bayes methods for assessing differential expression in microarray experiments. *Stat. Appl. Genet. Mol. Biol.* 3:e3.

Strauss, O. 2005. The retinal pigment epithelium in visual function. *Physiol. Rev.* 85:845–881. http://dx.doi.org/10.1152/physrev.00021.2004

Tarallo, V., Y. Hirano, B.D. Gelfand, S. Dridi, N. Kerur, Y. Kim, W.G. Cho, H. Kaneko, B.J. Fowler, S. Bogdanovich, et al. 2012. DICER1 loss and Alu RNA induce age-related macular degeneration via the NLRP3 inflammasome and MyD88. *Cell.* 149:847–859. http://dx.doi.org/10.1016/j.cell.2012.03.036

Townsend, M.J., P.G. Fallon, D.J. Matthews, H.E. Jolin, and A.N. McKenzie. 2000. T1/ST2-deficient mice demonstrate the importance of T1/ST2 in developing primary T helper cell type 2 responses. *J. Exp. Med.* 191:1069–1076. http://dx.doi.org/10.1084/jem.191.6.1069

Vander Lugt, B., A.A. Khan, J.A. Hackney, S. Agrawal, J. Lesch, M. Zhou, W.P. Lee, S. Park, M. Xu, J. DeVoss, et al. 2014. Transcriptional programming of dendritic cells for enhanced MHC class II antigen presentation. *Nat. Immunol.* 15:161–167. http://dx.doi.org/10.1038/ni.2795

Villarreal, D.O., M.C. Wise, J.N. Walters, E.L. Reuschel, M.J. Choi, N. Obeng-Adjei, J. Yan, M.P. Morrow, and D.B. Weiner. 2014. Alarmin IL-33 acts as an immunoadjuvant to enhance antigen-specific tumor immunity. *Cancer Res.* 74:1789–1800. http://dx.doi.org/10.1158/0008-5472.CAN-13-2729

Wu, T.D., and S. Nacu. 2010. Fast and SNP-tolerant detection of complex variants and splicing in short reads. *Bioinformatics.* 26:873–881. http://dx.doi.org/10.1093/bioinformatics/btq057